Revised Version

DESY 03-032
LTH 571
LU-ITP 2003/003
Edinburgh 2003/02

Nucleon electromagnetic form factors on the lattice and in chiral effective field theory

M. Göckeler,[1,2] T.R. Hemmert,[3] R. Horsley,[4] D. Pleiter,[5]
P.E.L. Rakow,[6] A. Schäfer,[2] and G. Schierholz[5,7]

(QCDSF collaboration)

[1] *Institut für Theoretische Physik, Universität Leipzig, D-04109 Leipzig, Germany*
[2] *Institut für Theoretische Physik, Universität Regensburg, D-93040 Regensburg, Germany*
[3] *Physik-Department, Theoretische Physik,*
Technische Universität München, D-85747 Garching, Germany
[4] *School of Physics, University of Edinburgh, Edinburgh EH9 3JZ, UK*
[5] *John von Neumann-Institut für Computing NIC,*
Deutsches Elektronen-Synchrotron DESY, D-15738 Zeuthen, Germany
[6] *Theoretical Physics Division, Department of Mathematical Sciences,*
University of Liverpool, Liverpool L69 3BX, UK
[7] *Deutsches Elektronen-Synchrotron DESY, D-22603 Hamburg, Germany*

(Dated: March 4, 2005)

arXiv:hep-lat/0303019 v2 4 Mar 2005

Abstract

We compute the electromagnetic form factors of the nucleon in quenched lattice QCD, using non-perturbatively improved Wilson fermions, and compare the results with phenomenology and chiral effective field theory.

PACS numbers: 11.15.Ha; 12.38.Gc; 13.40.Gp

Keywords: Lattice QCD; effective field theory; chiral extrapolation; nucleon electromagnetic form factors

I. INTRODUCTION

The measurements of the electromagnetic form factors of the proton and the neutron gave the first hints at an internal structure of the nucleon, and a theory of the nucleon cannot be considered satisfactory if it is not able to reproduce the form factor data. For a long time, the overall trend of the experimental results for small and moderate values of the momentum transfer q^2 could be described reasonably well by phenomenological (dipole) fits

$$\begin{aligned} G_e^p(q^2) &\sim \frac{G_m^p(q^2)}{\mu^p} \sim \frac{G_m^n(q^2)}{\mu^n} \\ &\sim \left(1 - q^2/m_D^2\right)^{-2} , \\ G_e^n(q^2) &\sim 0 \end{aligned} \tag{1}$$

with $m_D \sim 0.84\,\mathrm{GeV}$ and the magnetic moments

$$\mu^p \sim 2.79 \quad , \quad \mu^n \sim -1.91 \tag{2}$$

in units of nuclear magnetons. Recently, the form factors of the nucleon have been studied experimentally with high precision and deviations from this uniform dipole form have been observed, both at very small q^2 [1] and in the region above $1\,\mathrm{GeV}^2$ [2, 3].

It is therefore of great interest to derive the nucleon form factors from QCD. Since form factors are typical low-energy quantities, perturbation theory in terms of quarks and gluons is useless for this purpose and a non-perturbative method is needed. If one wants to avoid additional assumptions or models, one is essentially restricted to lattice QCD and Monte Carlo simulations. In view of the importance of nucleon form factors and the amount of experimental data available, it is surprising that there are only a few lattice investigations of form factors in the last years [4, 5].

In this paper we give a detailed account of our results for the nucleon form factors obtained in quenched Monte Carlo simulations with non-perturbatively $O(a)$-improved Wilson fermions. We shall pay particular attention to the chiral extrapolation and compare with formulae from chiral effective field theory previously used for studies of the magnetic moments. The plan of the paper is as follows. After a few general definitions and remarks in the next section we describe the lattice technology that we used in Sec. III. After commenting on our earlier attempts to perform a chiral extrapolation in Sec. IV, we investigate the quark-mass dependence of the form factors in more detail on a phenomenological basis in Sec. V. We

find that our data are in qualitative agreement with the recently observed deviations [2, 3] from the uniform dipole parametrization of the proton form factors. In Sec. VI we collect and discuss formulae from chiral effective field theory, which are confronted with our Monte Carlo results in Sec. VII. Our conclusions are presented in Sec. VIII. The Appendixes contain a short discussion of the pion mass dependence of the nucleon mass as well as tables of the form factors and of the corresponding dipole fits.

II. GENERALITIES

Experimentally, the nucleon form factors are measured via electron scattering. Because the fine structure constant is so small, it is justified to describe this process in terms of one-photon exchange. So the scattering amplitude is given by

$$T_{fi} = e^2 \bar{u}_e(k_e', s_e') \gamma_\mu u_e(k_e, s_e) \frac{1}{q^2} \langle p', s' | J^\mu | p, s \rangle \tag{3}$$

with the electromagnetic current

$$J^\mu = \frac{2}{3} \bar{u} \gamma^\mu u - \frac{1}{3} \bar{d} \gamma^\mu d + \cdots . \tag{4}$$

Here p, p' are the nucleon momenta, k_e, k_e' are the electron momenta, and s, s', ...are the corresponding spin vectors. The momentum transfer is defined as $q = p' - p$. With the help of the form factors $F_1(q^2)$ and $F_2(q^2)$ the nucleon matrix element can be decomposed as

$$\langle p', s' | J^\mu | p, s \rangle = \bar{u}(p', s') \left[\gamma_\mu F_1(q^2) + \mathrm{i} \sigma^{\mu\nu} \frac{q_\nu}{2M_N} F_2(q^2) \right] u(p, s) \tag{5}$$

where M_N is the mass of the nucleon. From the kinematics of the scattering process, it can easily be seen that $q^2 < 0$. In the following, we shall often use the new variable $Q^2 = -q^2$. We have $F_1(0) = 1$ (in the proton) as J is a conserved current, while $F_2(0)$ measures the anomalous magnetic moment in nuclear magnetons. For a classical point particle, both form factors are independent of q^2, so deviations from this behavior tell us something about the extended nature of the nucleon. In electron scattering, F_1 and F_2 are usually re-written in terms of the electric and magnetic Sachs form factors

$$\begin{aligned} G_e(q^2) &= F_1(q^2) + \frac{q^2}{(2M_N)^2} F_2(q^2) , \\ G_m(q^2) &= F_1(q^2) + F_2(q^2) , \end{aligned} \tag{6}$$

as then the (unpolarized) cross section becomes a linear combination of squares of the form factors.

Throughout the whole paper we assume flavor SU(2) symmetry. Hence we can decompose the form factors into isovector and isoscalar components. In terms of the proton and neutron form factors the isovector form factors are given by

$$\begin{aligned} G_e^v(q^2) &= G_e^p(q^2) - G_e^n(q^2)\,, \\ G_m^v(q^2) &= G_m^p(q^2) - G_m^n(q^2) \end{aligned} \tag{7}$$

such that

$$G_m^v(0) = G_m^p(0) - G_m^n(0) = \mu^p - \mu^n = \mu^v = 1 + \kappa_v \tag{8}$$

with μ^v (κ_v) being the isovector (anomalous) magnetic moment ~ 4.71 (3.71). In the actual simulations we do not work directly with these definitions when we calculate the isovector form factors. We use the relation

$$\begin{aligned} &\langle \text{proton}| \left(\tfrac{2}{3}\bar{u}\gamma^\mu u - \tfrac{1}{3}\bar{d}\gamma^\mu d\right) |\text{proton}\rangle - \langle \text{neutron}| \left(\tfrac{2}{3}\bar{u}\gamma^\mu u - \tfrac{1}{3}\bar{d}\gamma^\mu d\right) |\text{neutron}\rangle \\ &\qquad = \langle \text{proton}| \left(\bar{u}\gamma^\mu u - \bar{d}\gamma^\mu d\right) |\text{proton}\rangle \end{aligned} \tag{9}$$

and compute the isovector form factors from proton matrix elements of the current $\bar{u}\gamma^\mu u - \bar{d}\gamma^\mu d$ instead of evaluating the proton and neutron matrix elements of the electromagnetic current separately and then taking the difference. Similarly one could use the isoscalar current $\bar{u}\gamma^\mu u + \bar{d}\gamma^\mu d$ for the computation of isoscalar form factors, but we have not done so, since in the isoscalar sector there are considerable uncertainties anyway due to the neglected quark-line disconnected contributions.

III. LATTICE TECHNOLOGY

Using the standard Wilson gauge field action we have performed quenched simulations with $O(a)$-improved Wilson fermions (clover fermions). For the coefficient c_{SW} of the Sheikholeslami-Wohlert clover term we chose a non-perturbatively determined value calculated from the interpolation formula given in Ref. [6]. The couplings $\beta = 6/g^2$ and c_{SW}, the lattice sizes and statistics, the values of the hopping parameter κ (not to be confused with an anomalous magnetic moment) and the corresponding pion and nucleon masses (in

TABLE I: Simulation parameters, numbers of gauge field configurations used (# configs.) and masses.

β	c_{SW}	κ	c_V	Volume	# configs.	am_π	aM_N
6.0	1.769	0.1320	−0.331	$16^3 \times 32$	$O(450)$	0.5412(9)	0.9735(40)
6.0	1.769	0.1324	−0.331	$16^3 \times 32$	$O(550)$	0.5042(7)	0.9353(25)
6.0	1.769	0.1333	−0.331	$16^3 \times 32$	$O(550)$	0.4122(9)	0.8241(34)
6.0	1.769	0.1338	−0.331	$16^3 \times 32$	$O(500)$	0.3549(12)	0.7400(85)
6.0	1.769	0.1342	−0.331	$16^3 \times 32$	$O(700)$	0.3012(10)	0.7096(48)
6.0	1.769	$\kappa_c = 0.1353$					0.5119(67)
6.2	1.614	0.1333	−0.169	$24^3 \times 48$	$O(300)$	0.4136(6)	0.7374(21)
6.2	1.614	0.1339	−0.169	$24^3 \times 48$	$O(300)$	0.3565(8)	0.6655(28)
6.2	1.614	0.1344	−0.169	$24^3 \times 48$	$O(300)$	0.3034(6)	0.5963(29)
6.2	1.614	0.1349	−0.169	$24^3 \times 48$	$O(500)$	0.2431(7)	0.5241(39)
6.2	1.614	$\kappa_c = 0.1359$					0.3695(36)
6.4	1.526	0.1338	−0.115	$32^3 \times 48$	$O(200)$	0.3213(8)	0.5718(28)
6.4	1.526	0.1342	−0.115	$32^3 \times 48$	$O(100)$	0.2836(9)	0.5266(31)
6.4	1.526	0.1346	−0.115	$32^3 \times 48$	$O(200)$	0.2402(8)	0.4680(37)
6.4	1.526	0.1350	−0.115	$32^3 \times 48$	$O(300)$	0.1933(7)	0.4156(34)
6.4	1.526	0.1353	−0.115	$32^3 \times 64$	$O(300)$	0.1507(8)	0.3580(47)
6.4	1.526	$\kappa_c = 0.1358$					0.2800(53)

lattice units) are collected in Table I. As we are going to investigate nucleon properties, we want to determine the lattice spacing from the (chirally extrapolated) nucleon mass in order to ensure that the nucleon mass takes the correct value. (At the present level of accuracy, the difference between the nucleon mass in the chiral limit and the physical nucleon mass can be neglected.) Ideally we would use a formula from chiral perturbation theory for this purpose, e.g. Eq. (A1). Since there seems to be little difference between quenched and unquenched results at presently accessible quark masses it would make sense to apply this formula to our data. However, it turns out that it breaks down for pion masses above 600 MeV [7], where almost all of our results lie (see Fig. 1). (For a detailed discussion of a different approach see Ref. [8].) Hence we resort to a simple-minded phenomenological

procedure extrapolating our masses by means of the ansatz

$$(aM_N)^2 = (aM_N^0)^2 + b_2(am_\pi)^2 + b_3(am_\pi)^3 \tag{10}$$

for each β. This ansatz provides a very good description of the data [9]. The nucleon masses extrapolated to the critical hopping parameter κ_c in this way (on the basis of a larger set of nucleon masses) are also given in Table I. Whenever we give numbers in physical units the scale has been set by these chirally extrapolated nucleon masses.

In the last years it has become more popular to set the scale with the help of the force parameter r_0 [10]. While this choice avoids the problems related to the chiral extrapolation of the nucleon mass, it has the disadvantage that the physical value of r_0 is less precisely determined than the physical nucleon mass. Furthermore, as the present paper deals exclusively with nucleon properties it seemed to us more important to have the correct value in physical units for the mass of the particle studied when evaluating other dimensionful quantities like, e.g., radii. It is however interesting to note that the dimensionless product $r_0 M_N^0$ is to a good accuracy independent of the lattice spacing. Indeed, taking r_0 from Ref. [11] and multiplying by the chirally extrapolated nucleon masses given in Table I one finds $r_0 M_N^0 = 2.75$, 2.72, and 2.73 for $\beta = 6.0$, 6.2, and 6.4, respectively. Thus the scaling behavior of our results is practically the same for both choices of the scale.

In Fig. 1 we plot M_N^2 versus m_π^2 using the masses from Table I. The picture demonstrates that scaling violations in the masses are small. Moreover, we see that for $m_\pi < 600\,\mathrm{MeV}$ our extrapolation curve is quite close to the chiral perturbation theory curve (A1).

In order to compute nucleon masses or matrix elements we need suitable interpolating fields. For a proton with spatial momentum $\vec{p}$ the most obvious choice in terms of the quark fields $u(x)$ and $d(x)$ is

$$\begin{aligned} B_\alpha(t,\vec{p}) &= \sum_{x,\, x_4=t} \mathrm{e}^{-\mathrm{i}\vec{p}\cdot\vec{x}} \epsilon_{ijk} u_\alpha^i(x) u_\beta^j(x) (C\gamma_5)_{\beta\gamma} d_\gamma^k(x)\,, \\ \bar{B}_\alpha(t,\vec{p}) &= \sum_{x,\, x_4=t} \mathrm{e}^{\mathrm{i}\vec{p}\cdot\vec{x}} \epsilon_{ijk} \bar{d}_\beta^i(x) (C\gamma_5)_{\beta\gamma} \bar{u}_\gamma^j(x) \bar{u}_\alpha^k(x) \end{aligned} \tag{11}$$

with the charge conjugation matrix C (α, β, γ are Dirac indices, i, j, k are color indices). Note that we now switch from Minkowski space to Euclidean space.

In Eq. (11) all three quarks sit at the same point. Clearly, as protons are not point objects this is not the best thing to do, and with the above interpolating fields we run the risk that

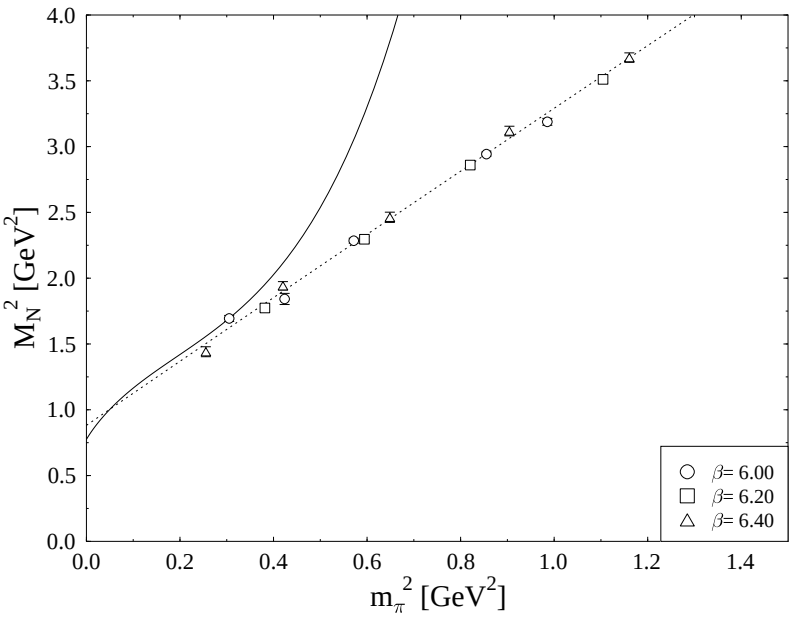

FIG. 1: Nucleon mass squared versus pion mass squared from the data in Table I. The dotted curve shows our phenomenological chiral extrapolation (Eq. (10)) for $\beta = 6.4$. The full curve corresponds to the chiral extrapolation derived from chiral perturbation theory (Eq. (A1)) with the parameters given in Appendix A.

the amplitudes of one-proton states in correlation functions might be very small making the extraction of masses and matrix elements rather unreliable. Therefore we employ two types of improvement: First we smear the sources and the sinks for the quarks in their time slices, secondly we apply a "non-relativistic" projection.

Our smearing algorithm (Jacobi smearing) is described in Ref. [12]. The parameters $N_{\rm smear}$, $\kappa_{\rm smear}$ used in the actual computations and the resulting smearing radii are given in Table II. A typical rms nucleon radius is about 0.8 fm, our smearing radii are about half that size.

The "non-relativistic" projection means that we replace each spinor by

$$\psi \to \psi^{NR} = \tfrac{1}{2}(1+\gamma_4)\psi \;,\; \bar{\psi} \to \bar{\psi}^{NR} = \bar{\psi}\tfrac{1}{2}(1+\gamma_4)\;. \tag{12}$$

This replacement leaves quantum numbers unchanged, but we would expect it to improve the overlap with baryons. Practically this means that for each baryon propagator we consider only the first two Dirac components. So we only have 2×3 inversions to perform rather

TABLE II: Smearing parameters for Jacobi smearing.

β	$N_{\rm smear}$	$\kappa_{\rm smear}$	$r_{\rm rms}$
6.0	50	0.21	$\sim 3.5a \sim 0.38\,$fm
6.2	100	0.21	$\sim 5.6a \sim 0.44\,$fm
6.4	150	0.21	$\sim 6.7a \sim 0.40\,$fm

than the usual 4×3 inversions – a saving of 50% in computer time.

The non-forward matrix elements required for the form factors are computed from ratios of three-point functions to two-point functions. The two-point function is defined as

$$C_2(t,\vec{p}\,) = \sum_{\alpha\beta} \Gamma_{\beta\alpha} \langle B_\alpha(t,\vec{p}\,) \bar{B}_\beta(0,\vec{p}\,)\rangle \tag{13}$$

with the spin projection matrix

$$\Gamma = \tfrac{1}{2}(1+\gamma_4)\,. \tag{14}$$

In the three-point function

$$C_3(t,\tau,\vec{p},\vec{p}\,') = \sum_{\alpha\beta} \Gamma_{\beta\alpha} \langle B_\alpha(t,\vec{p}\,) \mathcal{O}(\tau) \bar{B}_\beta(0,\vec{p}\,')\rangle \tag{15}$$

we have used, besides the matrix (14) corresponding to unpolarized matrix elements, also

$$\Gamma = \tfrac{1}{2}(1+\gamma_4)\mathrm{i}\gamma_5\gamma_2 \tag{16}$$

corresponding to polarization in the 2-direction. We then computed the ratios

$$R(t,\tau,\vec{p},\vec{p}\,') = \frac{C_3(t,\tau,\vec{p},\vec{p}\,')}{C_2(t,\vec{p}\,)} \times \left[\frac{C_2(\tau,\vec{p}\,) C_2(t,\vec{p}\,) C_2(t-\tau,\vec{p}\,')}{C_2(\tau,\vec{p}\,') C_2(t,\vec{p}\,') C_2(t-\tau,\vec{p}\,)} \right]^{1/2} . \tag{17}$$

If all time differences are sufficiently large, i.e. if $0 \ll \tau \ll t$, R is proportional to the (polarized or unpolarized) proton matrix element of the operator $\mathcal{O}$ with a known kinematical coefficient presented below.

For the electromagnetic form factors the operator to be studied is the vector current. In contrast to previous investigations [4, 5], which used the conserved vector current, we chose to work with the local vector current $\bar{\psi}(x)\gamma_\mu\psi(x)$. The local vector current has to be renormalized, because it is not conserved. It should also be improved so that its matrix elements have discretization errors of $O(a^2)$ only, which means that we use the operator

$$V_\mu = Z_V(1+b_V a m_q)\left[\bar{\psi}\gamma_\mu\psi + \mathrm{i}c_V a \partial_\lambda(\bar{\psi}\sigma_{\mu\lambda}\psi)\right] , \tag{18}$$

where m_q is the bare quark mass:

$$am_q = \frac{1}{2\kappa} - \frac{1}{2\kappa_c}\,. \tag{19}$$

We have taken Z_V and b_V from the parametrizations given by the ALPHA collaboration [13] (see also Ref. [14]). The improvement coefficient c_V has also been computed non-perturbatively [15]. The results can be represented by the expression [9]

$$c_V = -0.01225\,\frac{4}{3}\,g^2\frac{1-0.3113g^2}{1-0.9660g^2}\,, \tag{20}$$

from which we have calculated c_V (see Table I). In the limit $g^2 \to 0$ it agrees with perturbation theory [16]. Computing all these additional contributions in our simulations, we found the improvement terms to be numerically small. Note that the improvement coefficient c_{CVC} for the conserved vector current is only known to tree level so that a fully non-perturbative analysis would not be possible had we used the conserved vector current.

In order to describe the relation between the ratios we computed and the form factors let us call the ratio R for the μ-component of the renormalized vector current more precisely R_μ. Furthermore we distinguish the unpolarized case (spin projection matrix (14)) from the polarized case (spin projection matrix (16)) by a superscript. The (Minkowski) momentum transfer is given by

$$q^2 = -Q^2 = 2\left(M_N^2 + \vec{p}\cdot\vec{p}\,' - E_N(\vec{p})E_N(\vec{p}\,')\right) \tag{21}$$

with the nucleon energy

$$E_N(\vec{p}\,) = \sqrt{M_N^2 + \vec{p}^{\,2}}\,. \tag{22}$$

Using the abbreviation

$$A(\vec{p},\vec{p}\,')^{-1} = (-Q^2 - 4M_N^2)\sqrt{E_N(\vec{p}\,)(M_N + E_N(\vec{p}\,))E_N(\vec{p}\,')(M_N + E_N(\vec{p}\,'))} \tag{23}$$

we have

$$\begin{aligned} R_4^{\rm unpol}(t,\tau,\vec{p},\vec{p}\,') = A(\vec{p},\vec{p}\,')\Big[& G_e(Q^2)M_N\big(E_N(\vec{p}\,) + E_N(\vec{p}\,')\big) \\ & \times\big(\vec{p}\,'\cdot\vec{p} - (M_N + E_N(\vec{p}\,))(M_N + E_N(\vec{p}\,'))\big) \\ & + G_m(Q^2)\big((\vec{p}\,'\cdot\vec{p}\,)^2 - \vec{p}^{\,2}\vec{p}\,'^2\big)\Big]\,, \end{aligned} \tag{24}$$

$$R_4^{\rm pol}(t,\tau,\vec{p},\vec{p}\,') = A(\vec{p},\vec{p}\,')\mathrm{i}(p_1' p_3 - p_3' p_1)\Big[G_e(Q^2) M_N\big(E_N(\vec{p}\,) + E_N(\vec{p}\,')\big) + G_m(Q^2)\big(\vec{p}\,'\cdot\vec{p} - (M_N + E_N(\vec{p}\,))(M_N + E_N(\vec{p}\,'))\big)\Big]\,, \quad (25)$$

and for $j = 1,2,3$

$$R_j^{\rm unpol}(t,\tau,\vec{p},\vec{p}\,') = A(\vec{p},\vec{p}\,')\mathrm{i}\Big[G_e(Q^2) M_N\big(p_j + p_j'\big)\big((M_N + E_N(\vec{p}\,))(M_N + E_N(\vec{p}\,')) - \vec{p}\,'\cdot\vec{p}\big) + G_m(Q^2)\big(p_j(E_N(\vec{p}\,)\vec{p}\,'^2 - E_N(\vec{p}\,')\vec{p}\,'\cdot\vec{p}\,) + p_j'(E_N(\vec{p}\,')\vec{p}^{\,2} - E_N(\vec{p}\,)\vec{p}\,'\cdot\vec{p}\,)\big)\Big]\,, \quad (26)$$

$$R_j^{\rm pol}(t,\tau,\vec{p},\vec{p}\,') = A(\vec{p},\vec{p}\,')\Big[G_e(Q^2) M_N\big(p_j + p_j'\big)\big(p_1' p_3 - p_3' p_1\big) + G_m(Q^2)\big(M_N(p_2 + p_2')(\vec{p}\,'\times\vec{p}\,)_j + \big((M_N + E_N(\vec{p}\,))(M_N + E_N(\vec{p}\,')) - \vec{p}\,'\cdot\vec{p}\big)\sum_{k=1}^{3}\epsilon_{j2k}(p_k' E_N(\vec{p}\,) - p_k E_N(\vec{p}\,'))\big)\Big]\,. \quad (27)$$

Analogous expressions for the computation of the form factors F_1 and F_2 are obtained by inserting the definitions (6) in the above equations.

We have computed the ratios R in (17) for two choices of the momentum $\vec{p}$,

$$\frac{L}{2\pi}\vec{p} = \begin{pmatrix}0\\0\\0\end{pmatrix}\,,\ \begin{pmatrix}1\\0\\0\end{pmatrix}\,, \quad (28)$$

and eight choices of the vector $\vec{q} = \vec{p}\,' - \vec{p}$,

$$\frac{L}{2\pi}\vec{q} = \begin{pmatrix}0\\0\\0\end{pmatrix}\,,\ \begin{pmatrix}0\\-1\\0\end{pmatrix}\,,\ \begin{pmatrix}0\\-2\\0\end{pmatrix}\,,\ \begin{pmatrix}-1\\0\\0\end{pmatrix}\,,\ \begin{pmatrix}-2\\0\\0\end{pmatrix}\,,\ \begin{pmatrix}-1\\-1\\0\end{pmatrix}\,,\ \begin{pmatrix}-1\\-1\\-1\end{pmatrix}\,,\ \begin{pmatrix}0\\0\\-1\end{pmatrix}\,, \quad (29)$$

where L denotes the spatial extent of the lattice. In Fig. 2 we show two examples of these ratios plotted versus τ (for the unimproved operator). The final results for R have been determined by a fit with a constant in a suitable τ interval. The corresponding errors have been computed by a jackknife procedure. The values chosen for t and for the fit intervals are collected in Table III.

Generically, several combinations of the above momenta lead to the same Q^2, and several ratios R contain the form factors at this Q^2 with non-vanishing coefficients. Hence we determined $G_e(Q^2)$ and $G_m(Q^2)$ from an (uncorrelated) MINUIT fit of all these Rs with

TABLE III: Sink positions t and fit intervals (in τ) used for the extraction of the ratios R.

β	t	fit interval
6.0	13	[4,9]
6.2	17	[6,11]
6.4	23	[7,16]

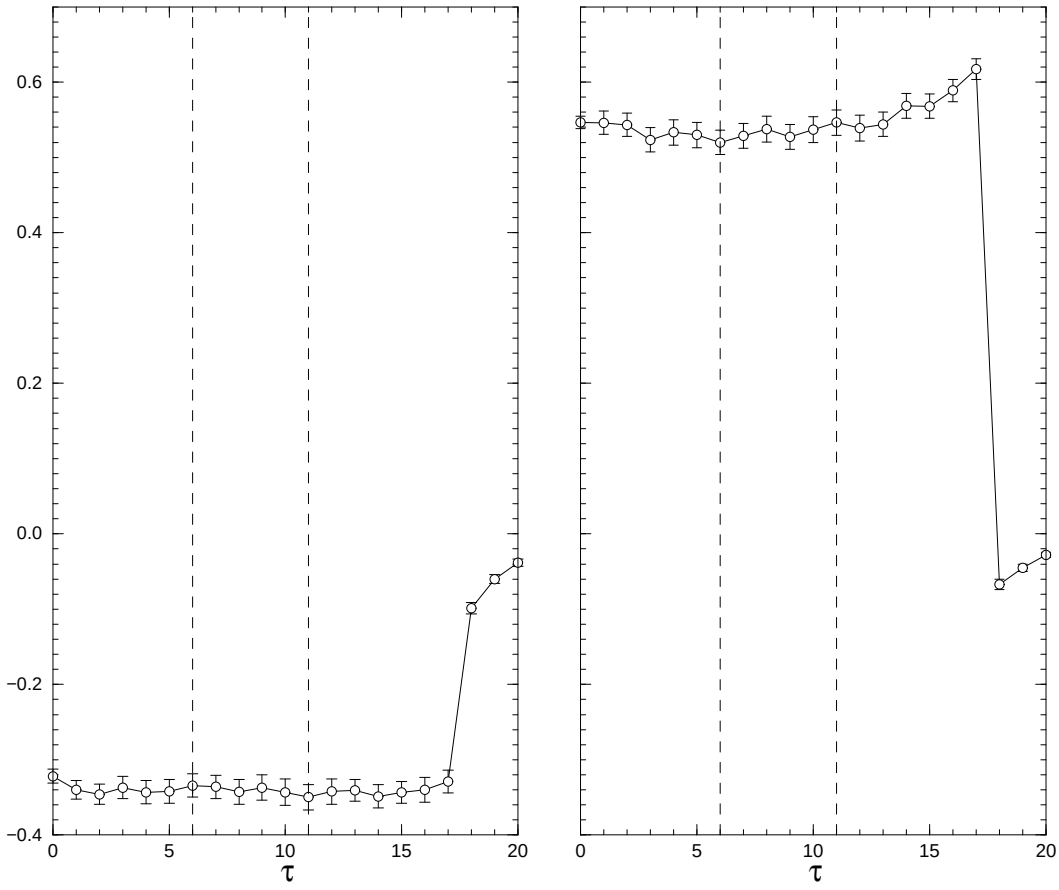

FIG. 2: The ratios $R_3^{\rm pol}$ (left) and $R_4^{\rm unpol}$ (right) plotted versus τ for $\beta = 6.2$, $\kappa = 0.1344$. Here $\vec{p} = \vec{0}$ and $\vec{q}$ is the fourth momentum in the list (29). The vertical dashed lines indicate the fit range for the extraction of the plateau value.

the corresponding expressions (24) - (27) omitting all data points where the error for R was larger than 25%. The results are collected in the tables in Appendix B. A missing entry indicates a case where the corresponding form factor could not be extracted, e.g. because we did not have sufficiently many Rs with less than 25% error.

The nucleon masses used can be found in Table I. The corresponding errors were, however, not taken into account when computing the errors of the form factors. Varying the nucleon masses within one standard deviation changed the form factors only by fractions of the quoted statistical error.

In general, the nucleon three-point functions consist of a quark-line connected contribution and a quark-line disconnected piece. Unfortunately, the quark-line disconnected piece is very hard to compute (for some recent attempts see Refs. [17, 18, 19]). Therefore it is usually neglected, leading to one more source of systematic uncertainty. However, in the case of exact isospin invariance the disconnected contribution drops out in non-singlet quantities like the isovector form factors. That is why the isovector form factors (Tables VIII - X) are our favorite observables. Nevertheless, we have also computed the proton form factors separately ignoring the disconnected contributions. The results are given in Tables XI - XIII. Regrettably, meaningful values of the electric form factor of the neutron could not be extracted from our data (for a more successful attempt see Ref. [20]). The results for the neutron magnetic form factor are collected in Tables XIV - XVI. Note that the isovector form factors have been computed directly (cf. Eq. (9)) and not as the difference of the proton and neutron form factors.

IV. CHIRAL EXTRAPOLATION: A FIRST ATTEMPT

The quark masses in our simulations are considerably larger than in reality leading to pion masses above 500 MeV. Hence we cannot compare our results with experimental data without performing a chiral extrapolation. In a first analysis of the proton results (see Refs. [21, 22]) we assumed a linear quark-mass dependence of the form factors. More precisely, we proceeded as follows.

Schematically, the relation between a ratio R (three-point function/two-point function) and the form factors G_e, G_m can be written in the form

$$R = \langle p'|J|p\rangle + \cdots = c_e G_e + c_m G_m \tag{30}$$

with known coefficients c_e, c_m for each data point characterized by the momenta, the quark mass, the spin projection and the space-time component of the current. Assuming a linear

quark-mass dependence of G_e and G_m we performed a 4-parameter fit,

$$R = c_e a_e(am_q) + c_e b_e + c_m a_m(am_q) + c_m b_m \,, \tag{31}$$

of all ratios R belonging to the same value of Q^2 in the chiral limit. The resulting form factors in the chiral limit are typically larger than the experimental data. They can be fitted with a dipole form, but the masses from these fits are considerably larger than their phenomenological counterparts [21, 22].

What could be the reason for this discrepancy? Several possibilities suggest themselves: finite-size effects, quenching errors, cut-off effects or uncertainties in the chiral extrapolation. The length L of the spatial boxes in our simulations is such that the inequality $m_\pi L > 4$ holds in all cases. Previous experience suggests that in the quenched approximation this is sufficient to exclude considerable distortions of the results due to the finite volume. This assumption is confirmed by simulations with Wilson fermions, where we have data on different volumes. Quenching errors are much more difficult to control. However, first simulations with dynamical fermions indicate that – for the rather heavy quarks we can deal with – the form factors do not change very much upon unquenching [22]. Having Monte Carlo data for three different lattice spacings (see Table I) we can test for cut-off effects in the chirally extrapolated form factors, but we find them to be hardly significant. So our chiral extrapolation ought to be reconsidered. Indeed, the chiral extrapolation of lattice data has been discussed intensively in the recent literature (see, e.g., Refs. [19, 20, 23, 24, 25, 26, 27, 28]) and it has been pointed out that the issue is highly non-trivial. Therefore we shall examine the quark-mass dependence of our form factors in more detail.

Ideally, one would like to identify a regime of parameters (quark masses in particular) where contact with chiral effective field theory (ChEFT) can be made on the basis of results like those presented for the nucleon form factors in Ref. [29]. Once the range of applicability of these low-energy effective field theories has been established, one can use them for a safe extrapolation to smaller masses. However, these schemes do not work for arbitrarily large quark masses (or pion masses), nor for arbitrarily large values of Q^2. In particular, the expressions for the form factors worked out in Ref. [29] can be trusted only up to $Q^2 \approx 0.4\,\mathrm{GeV}^2$ (see the discussion in Sec. VI A below) . Unfortunately, from our lattice simulations we only have data for values of Q^2 which barely touch the interval $0 < Q^2 < 0.4\,\mathrm{GeV}^2$. Therefore we shall try to describe the Q^2 dependence of the lattice data for each

quark mass by a suitable ansatz (of dipole type) and then study the mass dependence of the corresponding parameters. The fit ansatz will also serve as an extrapolation of the magnetic form factor down to $Q^2 = 0$. Since we cannot compute $G_m(0)$ directly, such an extrapolation is required anyway to determine the magnetic moment. (For a different method, which does not require an extrapolation, see Ref. [5].) In Sec. VII we shall come back to a comparison with ChEFT.

V. INVESTIGATING THE QUARK-MASS DEPENDENCE

The analysis of our form factor data sketched in Sec. IV yielded results in the chiral limit without much control over the approach to that limit. In this section we want to study the quark-mass dependence of the form factors more thoroughly. As already mentioned, to this end we have to make use of a suitable description of the Q^2 dependence.

Motivated by the fact that the experimentally measured form factors at small values of Q^2 can be described by a dipole form (cf. Eq. (1)) we fitted our data with the ansatz

$$\begin{aligned} G_l(Q^2) &= \frac{A_l}{(1+Q^2/M_l^2)^2} \quad , \quad l = e, m \,, \\ F_i(Q^2) &= \frac{A_i}{(1+Q^2/M_i^2)^2} \quad , \quad i = 1, 2 \,. \end{aligned} \tag{32}$$

In the case of the form factors G_e (F_1) we fixed $A_e = 1$ ($A_1 = 1$). Note that we do not require the dipole masses in the two form factors to coincide. Thus our ansatz can accomodate deviations of the ratio $G_m(0)G_e(Q^2)/G_m(Q^2)$ from unity as they have been observed in recent experiments [1, 2, 3].

Indeed, for all masses considered in our simulations the lattice data can be described rather well by a dipole ansatz. In Fig. 3 we show examples of our data (for $m_\pi = 0.648\,\mathrm{GeV}$) together with the dipole fits. The fit results are collected in Table XVII for the isovector form factors, in Table XVIII for the proton form factors and in Table XIX for the magnetic form factor of the neutron.

In Figs. 4, 5 we plot the isovector electric dipole mass M_e^v, the isovector magnetic dipole mass M_m^v and the isovector magnetic moment μ^v (extracted from the Sachs form factors) versus m_π. We make the following observations.

Scaling violations in the dipole masses seem to be smaller than the statistical accuracy, since the results do not show a definite trend as β grows from 6.0 to 6.4. For the magnetic

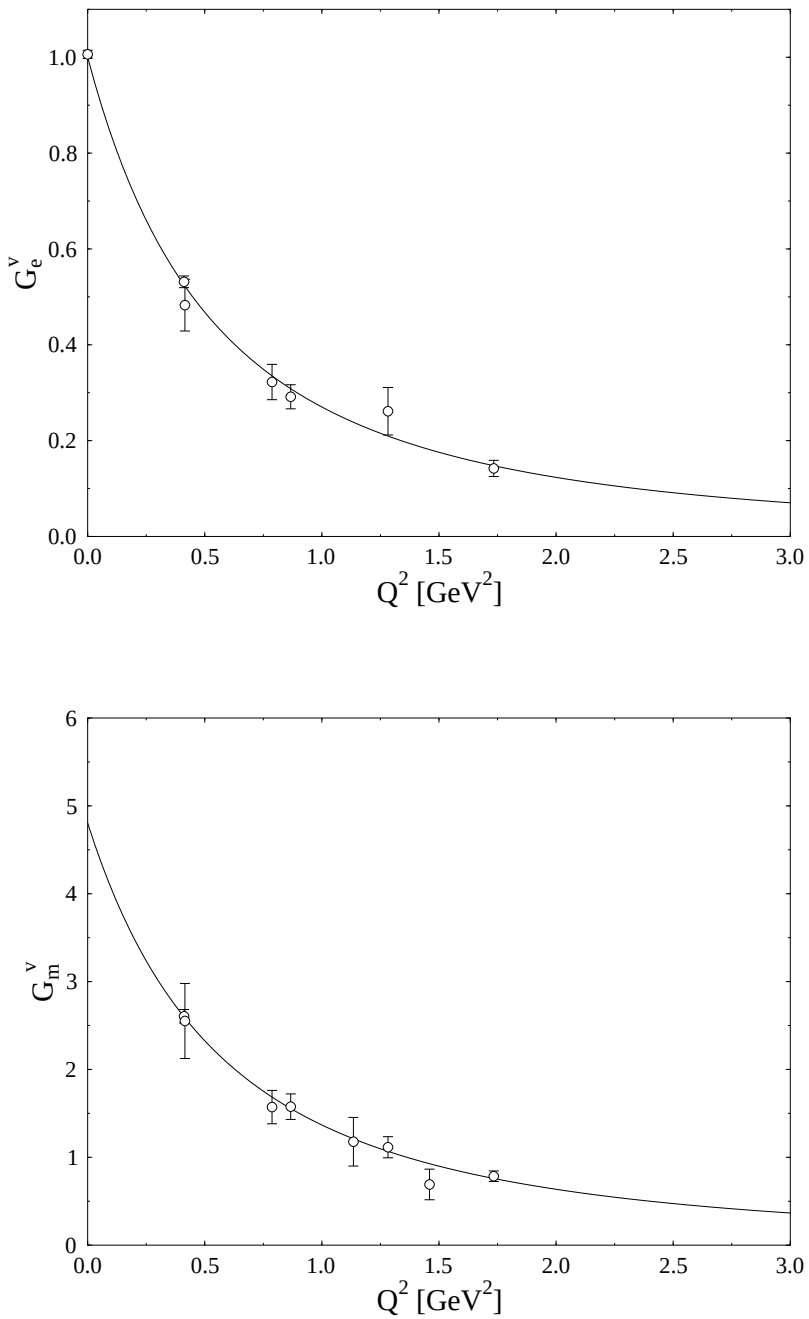

FIG. 3: Dipole fits of G_e^v data (top) and G_m^v data (bottom) at $\beta = 6.4$ and $m_\pi = 0.648\,\mathrm{GeV}$.

moments the situation is less clear. There might be some systematic shift, though not much larger than the statistical errors.

The electric dipole masses tend to become slightly smaller than the magnetic dipole masses as the pion mass decreases though it is not clear whether this difference is statistically

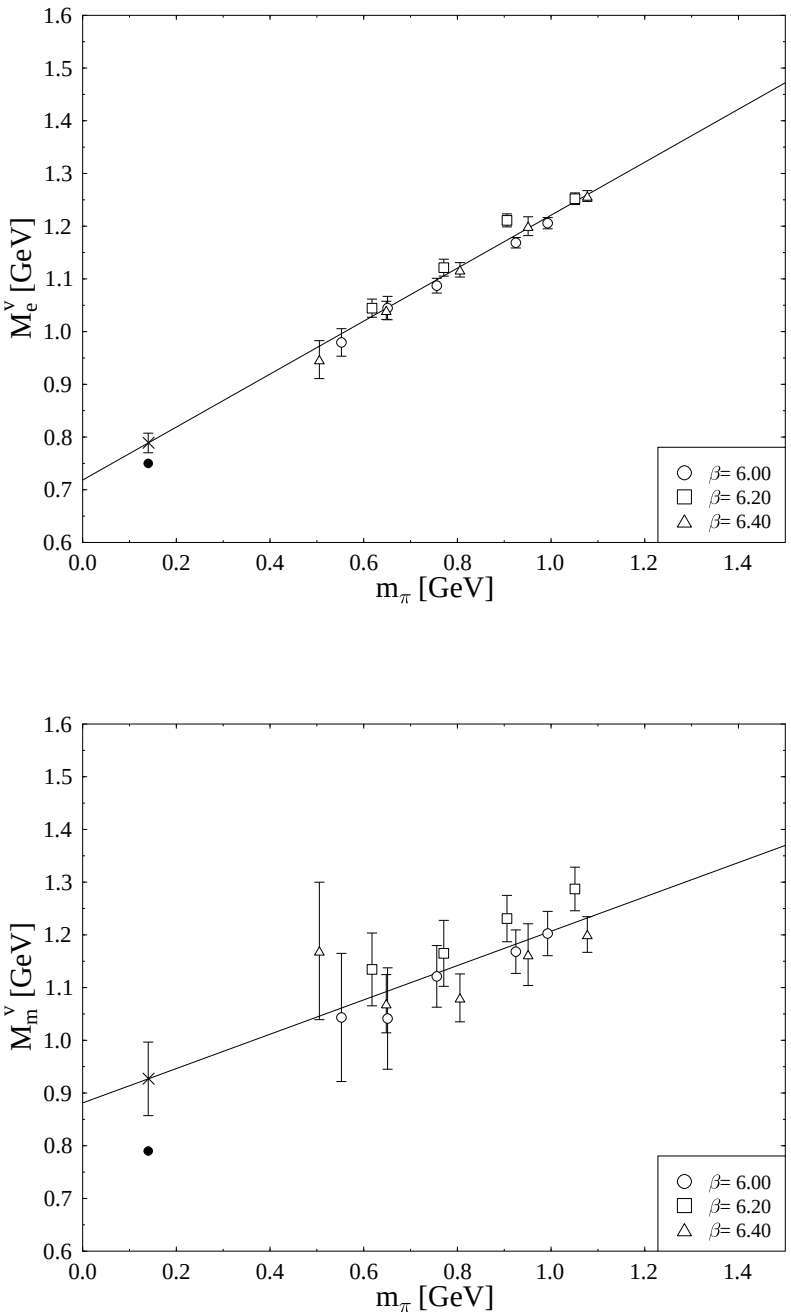

FIG. 4: Isovector dipole masses together with linear fits. The extrapolated value at the physical pion mass is marked by a cross. The solid circle indicates the phenomenological value computed from the radii given in Ref. [30].

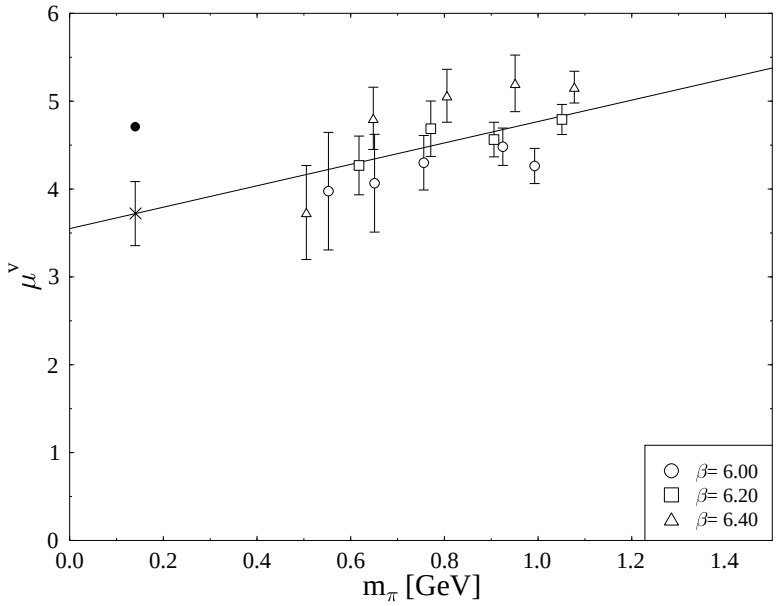

FIG. 5: Isovector magnetic moment together with a linear fit. The extrapolated value at the physical pion mass is marked by a cross. The solid circle indicates the experimental value.

significant. This behavior agrees qualitatively with the recent JLAB data [2, 3] for G_e/G_m in the proton (see Fig. 6 below).

The data for the electric dipole masses suggest a linear dependence on m_π. Therefore we could not resist temptation to perform linear fits of the dipole masses and moments (extracted from the Sachs form factors) in Tables XVII - XIX in order to obtain values at the physical pion mass. Of course, at some point the singularities and non-analyticities arising from the Goldstone bosons of QCD must show up and will in some observables lead to a departure from the simple linear behavior. It is however conceivable that this happens only at rather small pion masses (perhaps even only below the physical pion mass) and thus does not influence the value at the physical pion mass too strongly. One can try to combine the leading non-analytic behavior of chiral perturbation theory with a linear dependence on m_π^2 as it is expected at large quark mass in order to obtain an interpolation formula valid both at small and at large masses. Fitting our form factor data with such a formula one ends up remarkably close to the experimental results [28].

We performed our fits separately for each β value as well as for the combined data from

TABLE IV: Results at the physical pion mass from linear fits, separately for each β value as well as for the combined data. The experimental numbers for M_e^v and M_m^v were derived from the radii given in Ref. [30] (cf. Eq. (44) below).

	$\beta = 6.0$	$\beta = 6.2$	$\beta = 6.4$	combined	experiment
M_e^v [GeV]	0.78(3)	0.82(3)	0.77(3)	0.789(10)	0.75
M_m^v [GeV]	0.87(15)	0.94(13)	0.93(10)	0.93(7)	0.79
μ^v	3.9(8)	3.9(6)	3.9(6)	3.7(4)	4.71
M_e^p [GeV]	0.80(3)	0.84(3)	0.80(2)	0.807(15)	0.84
M_m^p [GeV]	0.93(15)	0.94(13)	0.92(10)	0.93(7)	0.84
μ^p	2.3(5)	2.4(4)	2.4(3)	2.3(2)	2.79
M_m^n [GeV]	0.83(16)	0.88(15)	0.91(11)	0.89(8)	0.84
μ^n	−1.6(4)	−1.6(3)	−1.5(3)	−1.47(17)	−1.91

all three β values. The results are presented in Table IV together with the experimental numbers. For the isovector dipole masses and the isovector magnetic moment the fit curves (from the joint fits for all β values) are plotted in Figs. 4, 5. The corresponding plots for the proton and neutron data look similar. In the case of the electric dipole mass, the extrapolated result lies remarkably close to the experimental value. For the magnetic dipole mass and the magnetic moment the agreement is less good, but still satisfactory in view of the relatively large statistical errors.

Using the dipole approximations of the proton form factors with the extrapolated dipole masses as given in the fifth column of Table IV we can now compare

$$\mu^p \frac{G_e^p(Q^2)}{G_m^p(Q^2)} = \frac{(1 + Q^2/(M_m^p)^2)^2}{(1 + Q^2/(M_e^p)^2)^2} \tag{33}$$

with the experimental data from Refs. [2, 3]. This is done in Fig. 6. Especially for the larger values of Q^2 we find good agreement, although the lattice data only cover the range $Q^2 < 2\,\mathrm{GeV}^2$ and for $Q^2 > 2\,\mathrm{GeV}^2$ the curve represents an extrapolation. It is perhaps not too surprising that the agreement improves as Q^2 grows: Larger Q^2 probe smaller distances inside the proton where the influence of the pion cloud, which is only insufficiently taken into account in the quenched approximation, is diminished.

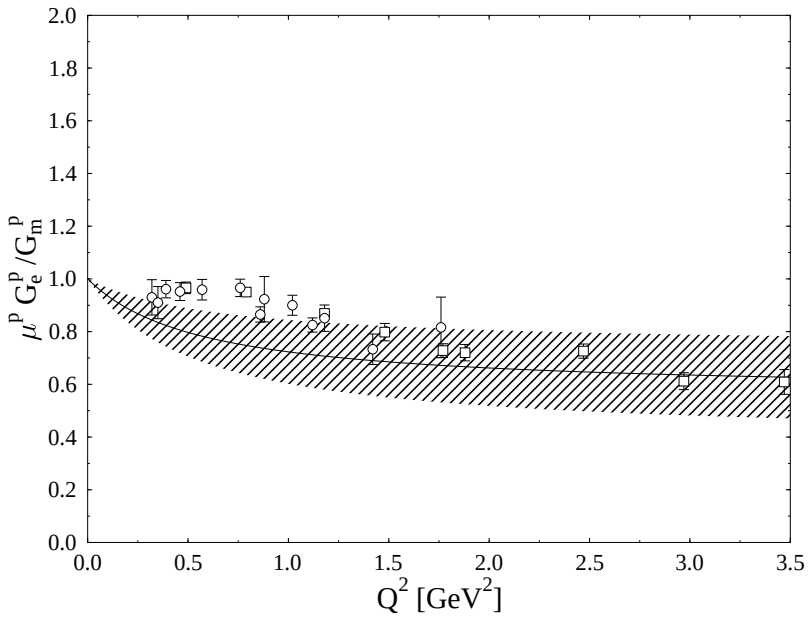

FIG. 6: The ratio $\mu^p G_e^p/G_m^p$ from the chirally extrapolated dipole fits of the proton form factors (curve) compared with the experimental data from Refs. [2] (squares) and [3] (circles). The error band (indicated by the hatched area) has been computed from the errors of the extrapolated dipole masses. For the experimental numbers only the statistical errors are shown.

VI. RESULTS FROM CHIRAL EFFECTIVE FIELD THEORY

A. From diagrams to form factors

For the comparison with ChEFT we choose the isovector form factors, because they do not suffer from the problem of quark-line disconnected contributions. Recently, a calculation for the quark-mass dependence of the isovector anomalous magnetic moment has been presented [24]. The authors employed a ChEFT with explicit nucleon and Δ degrees of freedom, called the Small Scale Expansion (SSE) [31]. It was argued [24] that the standard power-counting of ChEFT had to be changed to obtain a well-behaved chiral expansion – in particular, the leading isovector $N\Delta$ transition coupling c_V (not to be confused with the improvement coefficient used earlier) had to be included in the leading-order Lagrangian. For details we refer to Ref. [24]. The formula for the nucleon mass obtained in this framework is given in Eq. (A1). Here we extend this analysis from the magnetic moments to the Dirac and

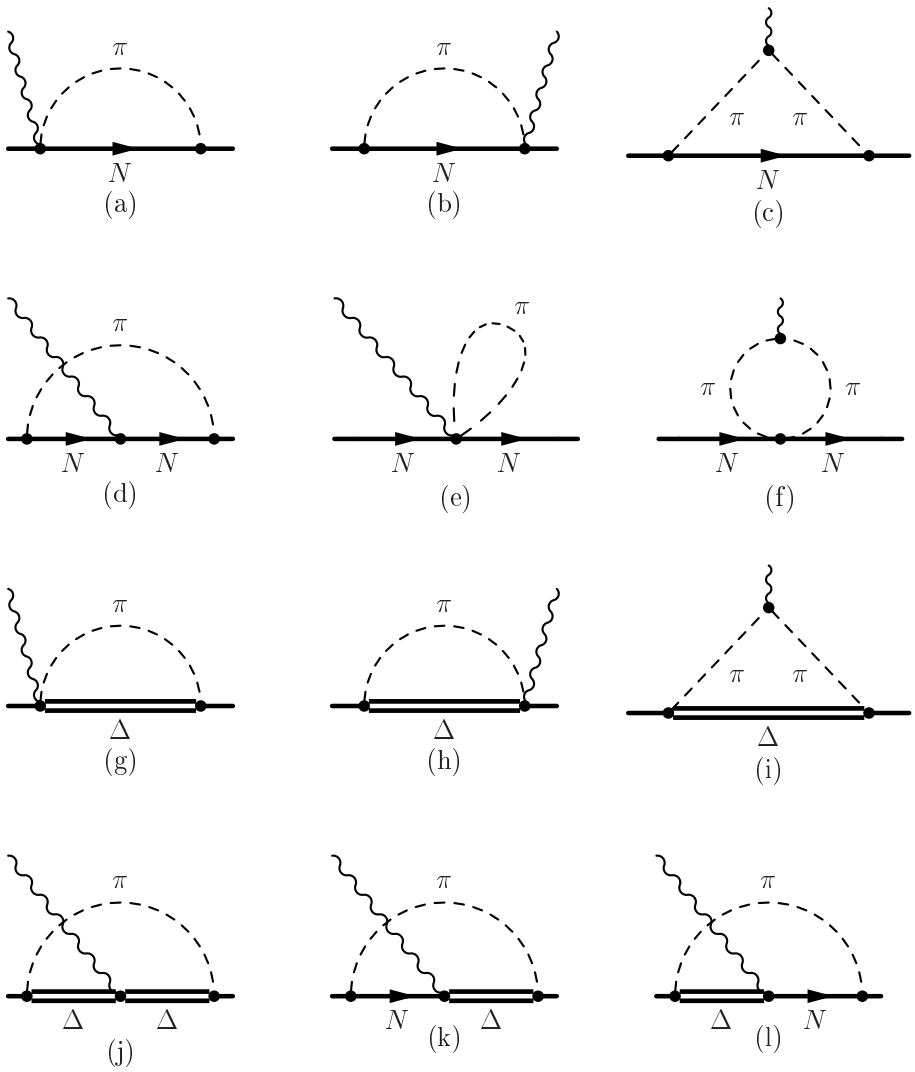

FIG. 7: One-loop diagrams in SSE contributing to the electromagnetic form factors. The wiggly line represents an external vector field.

Pauli form factors of the nucleon, utilizing the same Lagrangians and couplings as in [24]. To leading one-loop order ($\mathcal{O}(\epsilon^3)$ in SSE) 12 diagrams shown in Fig. 7 have to be evaluated in addition to the short-distance contributions. The calculation follows very closely the one presented in Ref. [29], where further technical details of form factor calculations in ChEFT are discussed. The main difference between our analysis here and Ref. [29] arises from the modified counting of c_V, leading to the additional diagrams (k) and (l) in Fig. 7. Evaluating all diagrams in the Breit frame, we identify the isovector form factors $F_1^v(q^2)$ and $F_2^v(q^2)$ via

the $\mathcal{O}(\epsilon^3)$ relation for the proton matrix element

$$\langle p_2|\left(\bar{u}\gamma_\mu u - \bar{d}\gamma_\mu d\right)|p_1\rangle_{\rm Breit} = \frac{e}{N_1 N_2}\,\bar{u}_v(r_2)\left[\left(F_1{}^v(q^2) + \frac{q^2}{4(M_N^0)^2}F_2{}^v(0) + \mathcal{O}(\epsilon^4)\right)v_\mu + \frac{1}{M_N^0}\left(F_1{}^v(0) + F_2{}^v(q^2) + \mathcal{O}(\epsilon^4)\right)[S_\mu, S_\nu]\,q^\nu\right]u_v(r_1) \quad (34)$$

written in Minkowski space notation. Here M_N^0 is the nucleon mass in the chiral limit and $u_v(r_i)$ denotes a nucleon spinor with the normalization N_i as given in Ref. [29]. The quantity S_μ denotes the Pauli-Lubanski spin-vector, $S_\mu = \frac{\rm i}{2}\gamma_5\sigma_{\mu\nu}v^\nu$. The four-vector v^μ ($v^2 = 1$) is connected to the usual four-momentum vector $p^\mu = M_N^0 v^\mu + r^\mu$, where r_μ is a soft momentum. Further details regarding calculations in this non-relativistic ChEFT can be found in Ref. [31].

Nevertheless we have to discuss some subtleties behind Eq. (34) to be able to compare the ChEFT results to lattice data. In (lattice) QCD a change in the quark mass does not only lead to a change in μ^v and κ_v, but at the same time also to a change in the nucleon mass. However, this variation of the nucleon mass – corresponding to a quark-mass dependent "magneton" – is not accounted for at the order in ChEFT we are working at, as can be seen from the presence of the nucleon mass in the chiral limit M_N^0 in Eq. (34). Hence, before comparing with the lattice results, we have to eliminate this effect. We do so by defining "normalized" magnetic moments which are measured relative to the *physical* mass of the nucleon $M_N^{\rm phys}$ and so are given in units of "physical" magnetons. These normalized magnetic moments can then be matched to the formulae from ChEFT with M_N^0 replaced by $M_N^{\rm phys}$.

We define the normalized magnetic moment by

$$\mu^v_{\rm norm} := \mu^v_{\rm lattice}\,\frac{M_N^{\rm phys}}{M_N^{\rm lattice}} = \frac{M_N^{\rm phys}}{M_N^{\rm lattice}} + \kappa_v^{\rm lattice}\,\frac{M_N^{\rm phys}}{M_N^{\rm lattice}}\,, \quad (35)$$

Correspondingly, we take for the normalized anomalous magnetic moment

$$\kappa_v^{\rm norm} := \kappa_v^{\rm lattice}\,\frac{M_N^{\rm phys}}{M_N^{\rm lattice}} \quad (36)$$

such that

$$\mu^v_{\rm norm} = \frac{M_N^{\rm phys}}{M_N^{\rm lattice}} + \kappa_v^{\rm norm}\,. \quad (37)$$

At higher orders in the chiral expansion, the quark-mass dependence of the nucleon mass will manifest itself in the matrix element (34), and the fits will have to be modified accordingly.

B. Form factors at $\mathcal{O}(\epsilon^3)$

For the isovector Dirac form factor we obtain

$$F_1^v(q^2) = 1 + \frac{1}{(4\pi F_\pi)^2}\left\{ q^2\left(\frac{68}{81}c_A^2 - \frac{2}{3}g_A^2 - 2B_{10}^{(r)}(\lambda)\right) + q^2\left(\frac{40}{27}c_A^2 - \frac{5}{3}g_A^2 - \frac{1}{3}\right)\log\left[\frac{m_\pi}{\lambda}\right] \right.$$
$$+ \int_0^1 dx\left[\frac{16}{3}\Delta^2 c_A^2 + m_\pi^2\left(3g_A^2 + 1 - \frac{8}{3}c_A^2\right) - q^2x(1-x)\left(5g_A^2 + 1 - \frac{40}{9}c_A^2\right)\right]\log\left[\frac{\tilde{m}^2}{m_\pi^2}\right]$$
$$+ \int_0^1 dx\left[\frac{32}{9}c_A^2 q^2 x(1-x)\frac{\Delta\log R(\tilde{m})}{\sqrt{\Delta^2-\tilde{m}^2}}\right]$$
$$\left. - \int_0^1 dx\ \frac{32}{3}c_A^2\Delta\left[\sqrt{\Delta^2-m_\pi^2}\log R(m_\pi) - \sqrt{\Delta^2-\tilde{m}^2}\log R(\tilde{m})\right]\right\} + \mathcal{O}(\epsilon^4)\,. \tag{38}$$

To the same order one finds

$$F_2^v(q^2) = \kappa_v(m_\pi) - g_A^2\frac{4\pi M_N}{(4\pi F_\pi)^2}\int_0^1 dx\left[\sqrt{\tilde{m}^2} - m_\pi\right]$$
$$+ \frac{32c_A^2 M_N\Delta}{9(4\pi F_\pi)^2}\int_0^1 dx\left[\frac{1}{2}\log\left[\frac{\tilde{m}^2}{4\Delta^2}\right] - \log\left[\frac{m_\pi}{2\Delta}\right]\right.$$
$$\left. + \frac{\sqrt{\Delta^2-\tilde{m}^2}}{\Delta}\log R(\tilde{m}) - \frac{\sqrt{\Delta^2-m_\pi^2}}{\Delta}\log R(m_\pi)\right] \tag{39}$$

for the isovector Pauli form factor, where we have used the abbreviations

$$R(m) = \frac{\Delta}{m} + \sqrt{\frac{\Delta^2}{m^2} - 1}\,, \quad \tilde{m}^2 = m_\pi^2 - q^2x(1-x)\,. \tag{40}$$

Furthermore, the isovector anomalous magnetic moment $\kappa_v(m_\pi)$ appearing in Eq. (39) is given by

$$\kappa_v(m_\pi) = \kappa_v^0 - \frac{g_A^2\, m_\pi M_N}{4\pi F_\pi^2} + \frac{2c_A^2\Delta M_N}{9\pi^2 F_\pi^2}\left\{\sqrt{1-\frac{m_\pi^2}{\Delta^2}}\log R(m_\pi) + \log\left[\frac{m_\pi}{2\Delta}\right]\right\}$$
$$- 8E_1^{(r)}(\lambda)M_N m_\pi^2 + \frac{4c_A c_V g_A M_N m_\pi^2}{9\pi^2 F_\pi^2}\log\left[\frac{2\Delta}{\lambda}\right] + \frac{4c_A c_V g_A M_N m_\pi^3}{27\pi F_\pi^2\Delta}$$
$$- \frac{8c_A c_V g_A\Delta^2 M_N}{27\pi^2 F_\pi^2}\left\{\left(1-\frac{m_\pi^2}{\Delta^2}\right)^{3/2}\log R(m_\pi) + \left(1-\frac{3m_\pi^2}{2\Delta^2}\right)\log\left[\frac{m_\pi}{2\Delta}\right]\right\} \tag{41}$$

to $\mathcal{O}(\epsilon^3)$. As already mentioned, to this order the nucleon mass M_N is a fixed number in the above expression, independent of the quark mass, and we shall later identify it with $M_N^{\rm phys}$. Note that Eq. (41) corresponds to case C in the terminology of Ref. [24]. Of course, it agrees with the result obtained in Ref. [24] because the magnetic moments are automatically contained in a calculation of the form factors, as can be seen from the diagrams of Fig. 7.

TABLE V: Empirical values of the parameters.

Parameter	Empirical value
g_A	1.267
c_A	1.125
F_π	0.0924 GeV
M_N	0.9389 GeV
Δ	0.2711 GeV
$\kappa_v^{\rm phys}$	3.71
$\kappa_s^{\rm phys}$	−0.12

The expressions (38) and (39) contain a number of phenomenological parameters: the pion decay constant F_π, the leading axial $N\Delta$ coupling c_A (denoted by $g_{\pi N\Delta}$ in Ref. [29]), the axial coupling of the nucleon g_A, the nucleon mass M_N and the $\Delta(1232)$-nucleon mass splitting $\Delta = M_\Delta - M_N$. In addition, there is one parameter not directly related to phenomenology, $B_{10}^{(r)}(\lambda)$. This counterterm at the renormalization scale λ parametrizes short-distance contributions to the Dirac radius discussed in the next subsection. Further parameters are encountered in the expression (41) for $\kappa_v(m_\pi)$: the isovector anomalous magnetic moment of the nucleon in the chiral limit κ_v^0, the leading isovector $N\Delta$ coupling c_V and the counterterm $E_1^{(r)}(\lambda)$, which leads to quark-mass dependent short-distance contributions to κ_v.

The only difference of the above results for the form factors compared to the formulae given in Ref. [29] lies in the mass dependence of $\kappa_v(m_\pi)$, as the two additional diagrams (l) and (k) of Fig. 7 do not modify the momentum dependence at $\mathcal{O}(\epsilon^3)$. The authors of Ref. [29] were only interested in the physical point $m_\pi = m_\pi^{\rm phys}$. Hence they fixed $\kappa_v(m_\pi^{\rm phys})$ to the empirical value $\kappa_v^{\rm phys} = 3.71$. In addition, one may determine the counterterm $B_{10}^{(r)}$ such that the phenomenological value of the isovector Dirac radius r_1^v is reproduced. This leads to $B_{10}^{(r)}(600\,\text{MeV}) = 0.34$. Using for the other parameters the phenomenological values as given in Table V and inserting (38) and (39) in (6) one gets a rather good agreement with the experimental Sachs form factors for values of Q^2 up to about $0.4\,\text{GeV}^2$, as exemplified in Fig. 8 by a comparison with the dispersion-theoretical description [30] of the isovector form factors. In addition we show in Fig. 8 the dipole approximations derived from the SSE formulae, which will be explained in Sec. VI C.

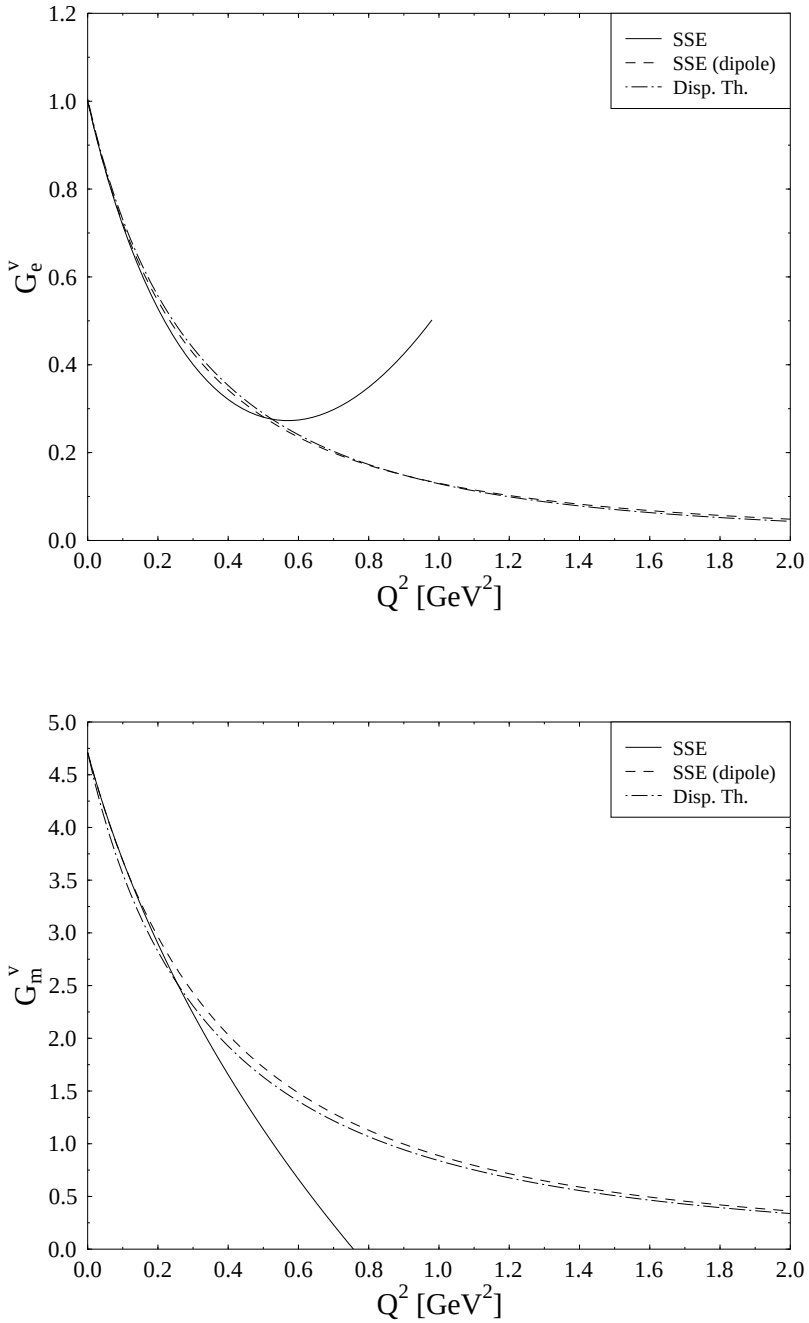

FIG. 8: Comparison of the dispersion-theoretical description of the isovector nucleon form factors with the SSE curves and the dipole approximations following from the SSE.

Here we want to study the quark-mass dependence of the form factors. Strictly speaking, in such a study all the parameters should be taken in the chiral limit. To order ϵ^3 in the SSE, the m_π dependence of F_1 and F_2 is then given by the expressions (38), (39), (41). For comparison we note that in Ref. [29] a function $\kappa_v(m_\pi)$ was found which corresponds to scheme B in the language of Ref. [24]. In this latter paper, scheme B was however shown to be insufficient to describe large-mass lattice data while scheme C turned out to work much better. Another recent calculation [32] of the nucleon form factors utilizes a relativistic framework for baryon chiral perturbation theory. However, as demonstrated in Ref. [24], it is not able to describe the mass dependence of the lattice data for κ_v. Therefore we shall not consider it for our fits.

Unfortunately, for most of the parameters the values in the chiral limit are only poorly known. That is why we shall usually work with the phenomenological numbers as given in Table V with the notable exception of the anomalous magnetic moment.

C. Form factor radii

From our lattice simulations we only have data for values of Q^2 which barely touch the interval $0 < Q^2 < 0.4\,\mathrm{GeV}^2$. Therefore a direct comparison with (38) and (39) does not make sense (although the Q^2 range in which the leading one-loop results of Eqs. (38) and (39) are applicable could depend on m_π) and we have to resort to another procedure, which exploits the dipole fits of our lattice form factors (see Sec. VII).

The dipole masses of the form factors are closely related to the radii r_i defined by the Taylor expansion of F_i around $q^2 = 0$:

$$F_i(q^2) = F_i(0)\left[1 + \frac{1}{6}\, r_i^2 q^2 + \mathcal{O}(q^4)\right] . \tag{42}$$

If one describes the Sachs form factors by the dipole formulae

$$\begin{aligned} G_e(q^2) &= \frac{1}{(1+Q^2/M_e^2)^2}\,, \\ G_m(q^2) &= \frac{G_m(0)}{(1+Q^2/M_m^2)^2}\,, \end{aligned} \tag{43}$$

the masses M_e and M_m are related to the above radii by

$$\frac{1}{M_e^2} = \frac{r_1^2}{12} + \frac{\kappa}{8M_N^2} \quad , \quad \frac{1}{M_m^2} = \frac{r_1^2 + \kappa\, r_2^2}{12(1+\kappa)}\,. \tag{44}$$

We note again that we do not demand the two dipole masses to be equal. Hence violations of the uniform dipole behavior can be accounted for.

From Eqs. (38) and (39) we can calculate the radii to $\mathcal{O}(\epsilon^3)$ in SSE. For the isovector Dirac radius one obtains

$$(r_1^v)^2 = -\frac{1}{(4\pi F_\pi)^2}\left\{1 + 7g_A^2 + \left(10g_A^2 + 2\right)\log\left[\frac{m_\pi}{\lambda}\right]\right\} - \frac{12B_{10}^{(r)}(\lambda)}{(4\pi F_\pi)^2} + \frac{c_A^2}{54\pi^2 F_\pi^2}\left\{26 + 30\log\left[\frac{m_\pi}{\lambda}\right] + 30\frac{\Delta}{\sqrt{\Delta^2 - m_\pi^2}}\log\left[\frac{\Delta}{m_\pi} + \sqrt{\frac{\Delta^2}{m_\pi^2} - 1}\right]\right\}. \quad (45)$$

The terms in the first bracket of Eq. (45) originate from Goldstone boson dynamics around a spin 1/2 nucleon (diagrams (a)-(f) in Fig. 7), the counter term $B_{10}^{(r)}(\lambda)$, which depends on the regularization scale λ, parametrizes short-distance contributions to the Dirac radius ("the nucleon core"), and the terms in the second bracket arise from Goldstone boson fluctuations around an intermediate $\Delta(1232)$ state (diagrams (g)-(l) in Fig. 7). Evaluating these terms at an intermediate regularization scale $\lambda = 600\,\mathrm{MeV}$ with the parameters given in Table V one obtains

$$(r_1^v)^2 = \left(0.41\,(N\pi) + 0.29\,(\Delta\pi)\right)\,\mathrm{fm}^2 - \frac{12\,B_{10}^{(r)}(600\,\mathrm{MeV})}{(4\pi F_\pi)^2}\,. \quad (46)$$

Note that the total result for $(r_1^v)^2$ depends only rather weakly on the regularization scale when λ varies between 500 and 700 MeV, as the scale dependence of the $N\pi$ and the $\Delta\pi$ contributions works in opposite direction.

Compared to the empirical value $(r_1^v)^2_{\mathrm{exp}} = 0.585\,\mathrm{fm}^2$ [30] the leading one-loop contributions from the Goldstone boson cloud tend to overestimate the Dirac radius (squared) by 20%. In Ref. [29] it was argued that one can always adjust the short-distance counter term $B_{10}^{(r)}(\lambda)$ to reproduce the physical isovector Dirac radius, e.g., $B_{10}^{(r)}(600\,\mathrm{MeV}) = 0.34$ works for the parameters of Table V.

Here, however, we do not want to follow this philosophy. It would mean that the leading contribution of the "nucleon core" to the square of the isovector Dirac radius becomes *negative*. We consider such a scenario as unphysical. In the following we therefore set $B_{10}^{(r)}(600\,\mathrm{MeV}) = 0$ (vanishing core contribution) and conclude that the $\mathcal{O}(\epsilon^3)$ SSE formula of Eq. (45) is not accurate enough to describe the quark-mass dependence of the isovector Dirac radius. Hence we can only expect a qualitative picture of the chiral extrapolation curve for this quantity, as shown in Sec. VII B.

For the leading one-loop isovector Pauli radius (squared) one obtains

$$(r_2^v)^2 = \frac{g_A^2 M_N}{8F_\pi^2 \kappa_v(m_\pi)\pi m_\pi} + \frac{c_A^2 M_N}{9F_\pi^2 \kappa_v(m_\pi)\pi^2\sqrt{\Delta^2 - m_\pi^2}} \log\left[\frac{\Delta}{m_\pi} + \sqrt{\frac{\Delta^2}{m_\pi^2} - 1}\right] + \frac{24 M_N}{\kappa_v(m_\pi)} B_{c2}\,. \tag{47}$$

The leading non-analytic quark-mass dependence $\sim m_\pi^{-1}$ is generated via the Goldstone boson cloud around a nucleon (diagrams (a)-(f) of Fig. 7), whereas the corresponding diagrams with an intermediate $\Delta(1232)$ state (diagrams (g)-(k) in Fig. 7) produce the remaining quark-mass dependence.

At leading one-loop order, in standard chiral counting one would not encounter the term $\propto B_{c2}$ (see Eq. (39)) which parametrizes the short-distance ("core") contributions to the Pauli radius analogous to $B_{10}^{(r)}(\lambda)$ in the Dirac radius (45). However, such a term – which should be present according to the physics reasoning alluded to above – is known to exist, see term no. 54 in Ref. [33]. Utilizing the parameters of Table V one finds (for the physical pion mass) the following contributions to the radius:

$$(r_2^v)^2 = \left(0.53\,(N\pi) + 0.09\,(\Delta\pi) + 0.24\,\mathrm{GeV}^3\, B_{c2}\right)\mathrm{fm}^2\,, \tag{48}$$

which without the "core term" $\propto B_{c2}$ are too small by 20% when compared to the empirical value $(r_2^v)^2_{\rm exp} = 0.797\,\mathrm{fm}^2$ [30]. Setting $B_{c2} = 0.74\,\mathrm{GeV}^{-3}$ for the physical parameters considered here (see Table V) one can reproduce the dispersion theoretical result with a *positive* core contribution. We shall study the chiral extrapolation function of $(r_2^v)^2$ with and without this core term in Sec. VII B to test whether our physical intuition regarding this structure holds true.

The radii (45) and (47) display much fewer quark-mass dependent terms than $\kappa_v(m_\pi)$ in Eq. (41) though all three quantities are calculated to the same $\mathcal{O}(\epsilon^3)$ accuracy in SSE. This seems to have its origin in the fact that one has to take out a factor of q^2 from the $\mathcal{O}(\epsilon^3)$ expression for the form factors in Eqs. (38), (39) in order to obtain the radius, leaving only a few possible structures for quark-mass dependent terms at this order. From the point of view of ChEFT it is therefore more involved to get the quark-mass dependence of radii under control than it is to study the quark-mass dependence of the form factors at $q^2 = 0$. In Sec. VII we shall compare the ChEFT formulae with the lattice data.

Even without the additional core term in Eq. (47) the dipole formulae with the above expressions for the radii reproduce the dispersion-theoretical form factors quite accurately

TABLE VI: Fit values from fits of Eqs. (41) and (49) to lattice data.

Parameter	Value from Ref. [24]
κ_v^0	5.1(4)
c_V	$-2.26(6)\,\mathrm{GeV}^{-1}$
$E_1^{(r)}(0.6\,\mathrm{GeV})$	$-4.93(10)\,\mathrm{GeV}^{-3}$
κ_s^0	-0.11
E_2	$0.074\,\mathrm{GeV}^{-3}$

for small and moderate values of Q^2 as can be seen from the dashed curves in Fig. 8. This observation constitutes a further argument in favor of our dipole fits. Empirical isovector dipole masses can be computed from the phenomenological isovector radii. One finds $M_e^v = 0.75\,\mathrm{GeV}$ and $M_m^v = 0.79\,\mathrm{GeV}$.

A final remark concerns the applicability of the above formulae to quenched data. Obviously, standard ChEFT presupposes the presence of sea quarks. However, as first unquenched simulations show, there is little difference between quenched and unquenched results at presently accessible quark masses. It is therefore not unreasonable to compare (38), (39) and (41) with quenched data. Alternatively, one could try to develop quenched chiral perturbation theory for the form factors. For first attempts see, e.g., Refs. [19, 34]. On the other hand, the size of our quark masses may lead to doubts on the applicability of one-loop ChEFT results. Only further investigations can clarify this issue. Here we simply try to find out how far we can get with the available formulae.

VII. COMPARISON WITH CHIRAL EFFECTIVE FIELD THEORY

A. Comparison with previous extrapolations for $\kappa_v(m_\pi)$

Hemmert and Weise [24] fitted lattice results for the normalized isovector magnetic moment μ_v^{norm} with the $\mathcal{O}(\epsilon^3)$ formula (41) using κ_v^0, c_V and $E_1^{(r)}(\lambda)$ as fit parameters and fixing the other parameters at their phenomenological values (see Table V). Their fit yielded a rather strong m_π dependence of μ_v^{norm} for small m_π. The values they obtained for their fit parameters are given in Table VI. A similarly strong m_π dependence had already been

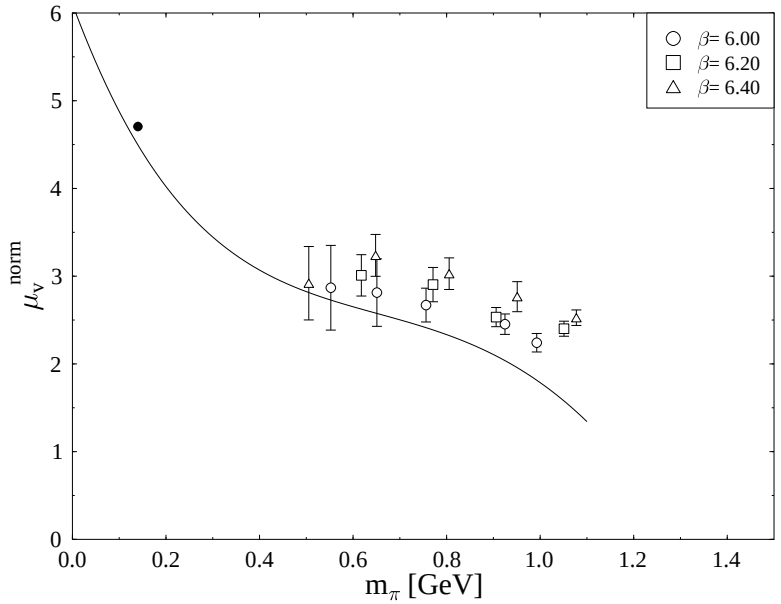

FIG. 9: Our results for the isovector (normalized) magnetic moments compared with the SSE extrapolation curve of Ref. [24]. The solid circle represents the experimental value of μ_v.

observed in Refs. [25, 26] for the magnetic moments of the proton and the neutron. In Fig. 9 we plot our data together with the curve corresponding to the fit of Ref. [24]. The comparison indicates that the data used in Ref. [24] lie somewhat below ours.

B. Combined fits

The results of Ref. [24] show that using the SSE it is possible to connect the experimental value of the magnetic moment with the lattice data. This raises the question whether one could not obtain a similarly good description of the radii by fitting the SSE expression to the simulation results. From the point of view of ChEFT the mass dependence of the Dirac and Pauli radius is much simpler to discuss than that of the analogous Sachs quantities. Hence we shall base our analysis on r_1^v and r_2^v instead of M_e^v and M_m^v. Note, however, that the numerical data in the following discussion are taken from the dipole fits of the Sachs form factors.

Because cut-off effects seem to be small we fitted the results from all three β values together taking into account all data points with $m_\pi < 1\,\mathrm{GeV}$. We kept F_π, M_N, c_A and Δ

TABLE VII: Results of a combined fit (with and without core term) of isovector Pauli radii and anomalous magnetic moments.

Parameter	Fitted value	Fitted value without core term
κ_v^0	5.1(8)	4.5(9)
c_V	$-2.3(5)\,\mathrm{GeV}^{-1}$	$-2.5(6)\,\mathrm{GeV}^{-1}$
$E_1^{(r)}(0.6\,\mathrm{GeV})$	$-4.8(8)\,\mathrm{GeV}^{-3}$	$-5.1(9)\,\mathrm{GeV}^{-3}$
B_{c2}	$0.41(4)\,\mathrm{GeV}^{-3}$	$0.0\,\mathrm{GeV}^{-3}$
χ^2	19.2	185.9

at their phenomenological values (see Table V), fixed the renormalization scale λ at 0.6 GeV and chose $B_{10}^{(r)}(0.6\,\mathrm{GeV}) = 0$ for the reason explained in Sec. VI C. Furthermore, we set $g_A = 1.2$, which is the value in the chiral limit obtained in a recent ChEFT analysis [35] of quenched lattice data. This leaves us with four fit parameters: κ_v^0, c_V, $E_1^{(r)}(0.6\,\mathrm{GeV})$ and B_{c2}. As the Dirac radius r_1^v is independent of these parameters, we performed a simultaneous fit of $(r_2^v)^2(m_\pi)$ and $\kappa_v^{\mathrm{norm}}(m_\pi)$. The results are collected in the second column of Table VII. Plots of our data together with the fit curves are shown in Figs. 10, 11. Leaving out the core term in r_2^v, i.e. setting $B_{c2} = 0$, leads to the parameter values given in the third column of Table VII. The corresponding curves are shown as dashed lines in the figures.

The lattice data for the isovector anomalous magnetic moment are very well described by the chiral extrapolation curve, in particular if one allows for a (small) core contribution via B_{c2}. Interestingly, the chiral extrapolation function comes rather close to the physical point, although the lightest lattice points are quite far from the physical world and large curvature is required. Moreover, the chiral limit value κ_v^0 and the values of the other two fit parameters $E_1^{(r)}$ and c_V in the second column of Table VII compare astonishingly well with the numbers found in Ref. [24] (see Table VI) providing us with some confidence in their determination. The lattice data for the isovector Pauli radius (squared) are also reasonably well described by the chiral extrapolation function of Eq. (47), at least for pion masses below 800 MeV. The effect of the finite core size of the nucleon (parametrized via B_{c2}) is more visible in this quantity than in κ_v. While the phenomenological value at the physical point is missed by our central curve for $r_2^v(m_\pi)$, it would lie within the error band, given the

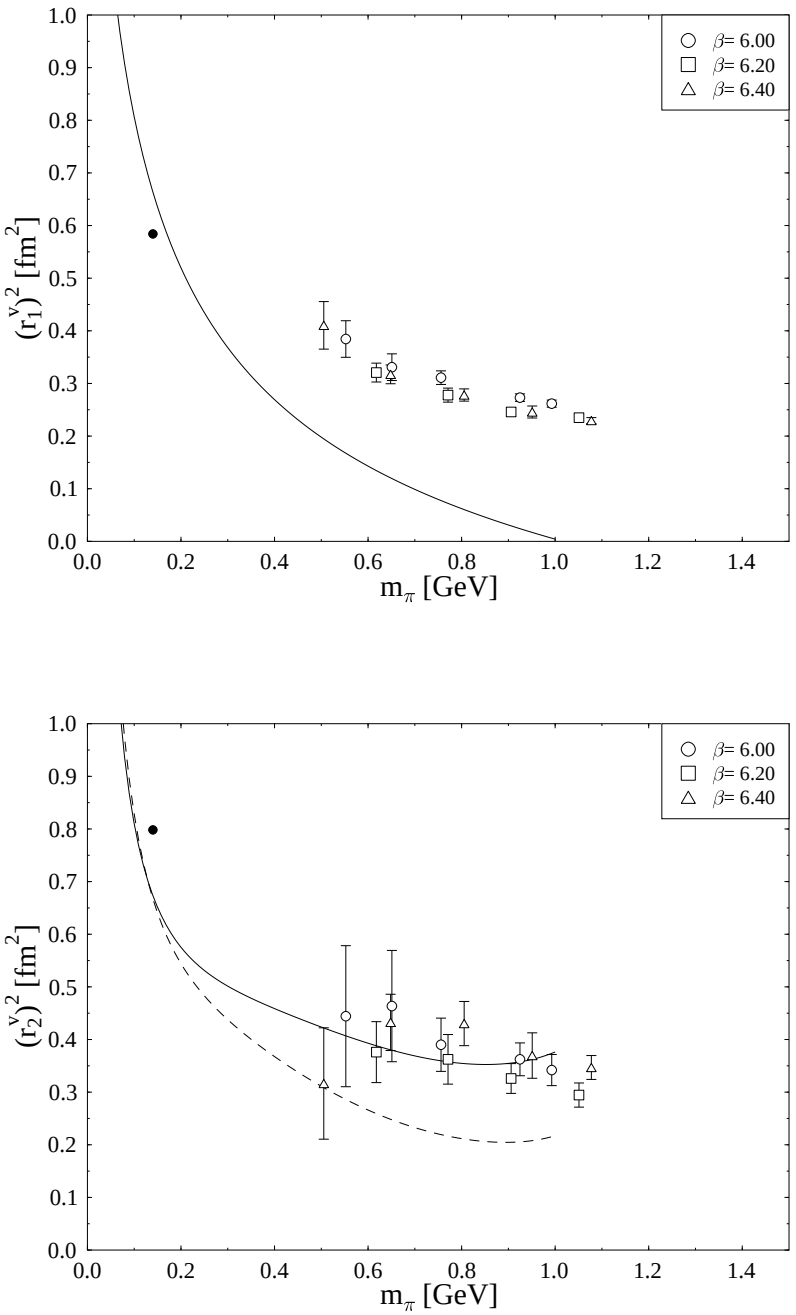

FIG. 10: Isovector radii compared with fit curves. For the fit parameters see Table VII. The dashed line corresponds to the fit without core term. The solid circles represent the experimental values.

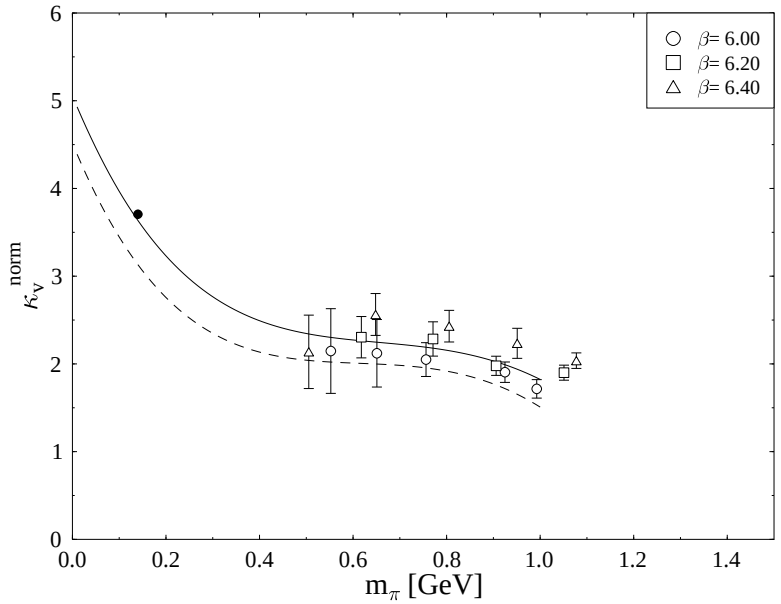

FIG. 11: Isovector (normalized) anomalous magnetic moments compared with (combined) fit. For the fit parameters see Table VII. The dashed line corresponds to the fit without core term. The solid circle represents the experimental value of κ_v.

relatively large errors of the fit parameters. We note that the $1/m_\pi$ chiral singularity shows up rather strongly, dominating the curvature out to pion masses around 0.3 GeV.

While our generalization of the ChEFT analysis of Ref. [24] describes the "magnetic" quantities κ_v and r_2^v reasonably well, it is not successful for the isovector Dirac radius. As can be seen in Fig. 10, the chiral extrapolation function drops too fast with m_π and even reaches zero around $m_\pi = 1\,\mathrm{GeV}$. Remember that Dirac radius data were not included in the fit and the curve shown corresponds to the "no-core term" scenario with $B_{10}^{(r)}(\lambda = 0.6\,\mathrm{GeV}) = 0$. One could improve the agreement between the lattice data and the chiral extrapolation curve by allowing $B_{10}^{(r)}$ to provide a positive core contribution, which would shift the curve upwards towards the data. However, this would result in extremely large values for $(r_1^v)^2$ at the physical point, as the shape is not modified by $B_{10}^{(r)}$. On the other hand, the simulation data themselves look completely reasonable, indicating that for pion masses around 1 GeV, for which the pion cloud should be considerably reduced, the square of the Dirac radius of the nucleon has shrunk to $\approx 0.25\,\mathrm{fm}^2$, less than half of the value at the physical point. One

reason for this failure of Eq. (45) might lie in important higher order corrections in ChEFT which could soften the strong m_π dependence originating from the chiral logarithm.

Nevertheless, one should also not forget that here we are dealing with a quenched simulation. Given that $(r_1^v)^2$ at the physical point is nearly completely dominated by the pion cloud (for low values of λ, cf. Eq. (46)) it is conceivable that the Dirac radius of the nucleon might be sensitive to the effects of (un)quenching. We therefore conclude that especially for r_1^v a lot of work remains to be done, both on the level of ChEFT, where the next-to-leading one-loop contributions need to be evaluated, as well as on the level of the simulations, where a similar analysis as the one presented here has to be performed based on fully dynamical configurations.

Of course, one can think of alternative fit strategies, which differ by the choice of the fixed parameters. For example, one might leave also c_A and Δ free in addition to the four parameters used above. In this (or a similar) way it is possible to force the fit through the data points for $(r_1^v)^2$ also, but then the physical point is missed by a considerable amount. So we must conclude that at the present level of accuracy the SSE expression for the Dirac radius is not sufficient to connect the Monte Carlo data in a physically sensible way with the phenomenological value.

C. Beyond the isovector channel

While ChEFT (to the order considered in Ref. [24]) yields the rather intricate expression (41) for the quark-mass dependence of the isovector anomalous magnetic moment, the analogous expression for the isoscalar anomalous magnetic moment $\kappa_s = \kappa_p + \kappa_n$ of the nucleon is much simpler,

$$\kappa_s(m_\pi) = \kappa_s^0 - 8E_2 M_N m_\pi^2 \,, \tag{49}$$

because the Goldstone boson contributions to this quantity only start to appear at the two-loop level [36]. The new counterterm E_2 parametrizes quark-mass dependent short-distance contributions to κ_s. The error bars of the lattice data are quite large compared to the small isoscalar anomalous magnetic moment. Therefore, any analysis based on (49) and the present lattice results must be considered with great caution, the more so, since the lattice data are also afflicted with the problem of the disconnected contributions. In spite of all these caveats, we now turn to a discussion of the magnetic moments and combinations of

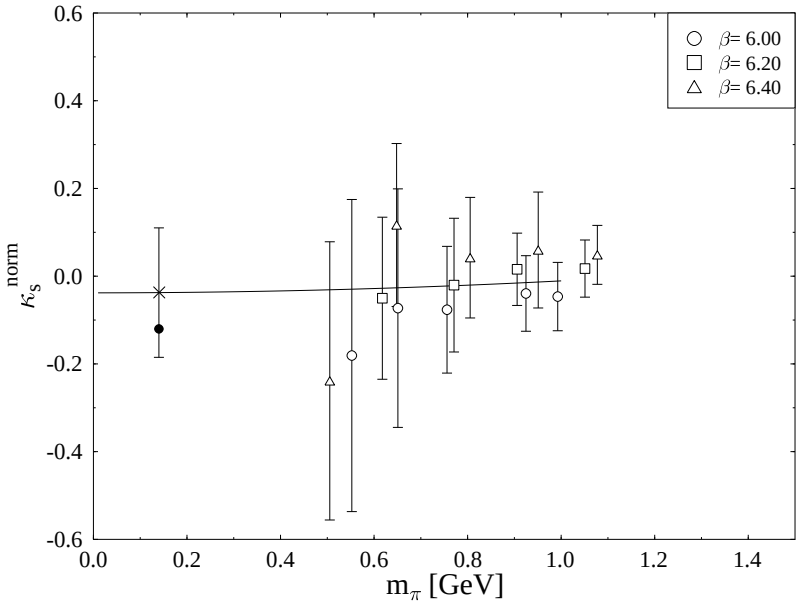

FIG. 12: Isoscalar (normalized) anomalous magnetic moments compared with SSE fit. The solid circle represents the experimental value of κ_s. The cross with the attached error bar shows the value at $m_\pi^{\rm phys}$.

them which are not purely isovector quantities.

In Fig. 12 we present the normalized values of κ_s together with a fit using Eq. (49). The values of κ_s have been computed as $\kappa_p + \kappa_n$ from the proton and neutron dipole fits of G_m, and the errors have been determined by error propagation. We obtain $\kappa_s^0 = -0.04(15)$ and $E_2 = -0.004(25)\,\mathrm{GeV}^{-3}$. These numbers are to be compared with the fit parameters from Ref. [24] given in Table VI. The large statistical errors make definite statements difficult.

Having determined $\kappa_v(m_\pi)$ as well as $\kappa_s(m_\pi)$ we can now discuss the chiral extrapolation of proton and neutron data separately. For κ_v^0, c_V, $E_1^{(r)}$, B_{c2} we choose the values given in the second column of Table VII together with $g_A = 1.2$, while for κ_s^0 and E_2 we take the numbers given above and the remaining parameters are fixed at their physical values (see Table V).

In Fig. 13 we compare the resulting extrapolation functions with the lattice results for the anomalous magnetic moments. The extrapolation functions are surprisingly well behaved. Despite the large gap between $m_\pi^{\rm phys}$ and the lowest data point and the substantial curvature

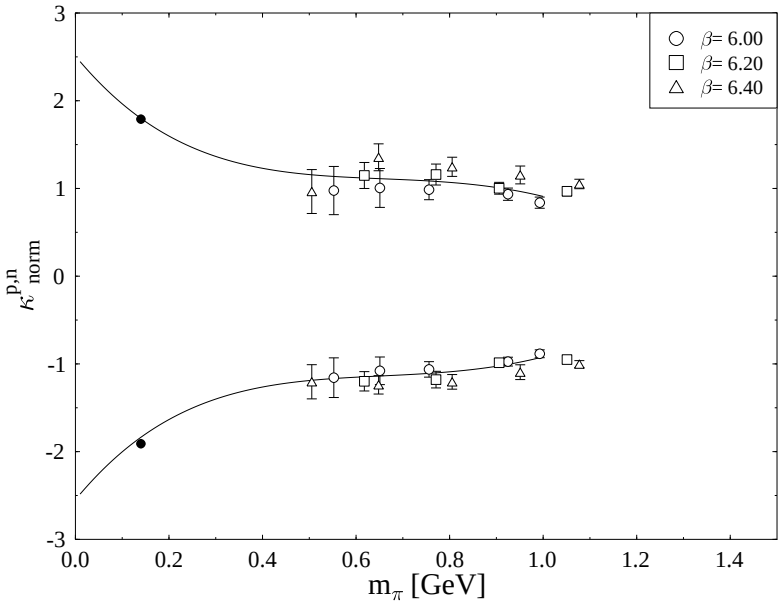

FIG. 13: Anomalous magnetic moments of proton and neutron (normalized) with chiral extrapolation curves. The solid circles represent the experimental values.

involved they extrapolate to the physical point and to the chiral limit in a very sensible way.

Finally, we want to compare our results with the predictions from the constituent quark model. Such comparisons are usually performed for ratios of observables to avoid normalization problems. Under the assumption that the constituent quark mass $m_q = m_u \approx m_d$ is equal to $M_N/3$ also for varying m_q, one obtains the well-known SU(6) result

$$\frac{\mu^p}{\mu^n} = \frac{\mu^p_{\rm norm}}{\mu^n_{\rm norm}} = -\frac{3}{2} \tag{50}$$

and similarly

$$\frac{\kappa_p}{\kappa_n} = \frac{\kappa_p^{\rm norm}}{\kappa_n^{\rm norm}} = -1\,. \tag{51}$$

In Fig. 14 we show the ratio of the anomalous magnetic moments κ_p/κ_n, which is identical to the ratio of the normalized anomalous magnetic moments, as a function of the pion mass. The lattice data and our extrapolation function stay rather close to the static SU(6) quark model value of -1 in the mass range considered here.

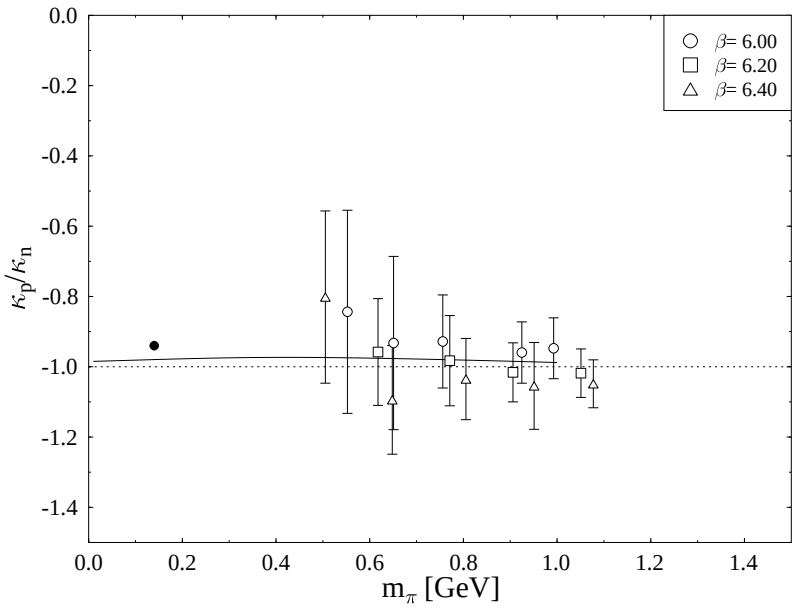

FIG. 14: The ratio κ_p/κ_n (identical to the ratio of the normalized anomalous magnetic moments) with chiral extrapolation curve. The dotted line shows the value -1.0 predicted by the non-relativistic quark model. The solid circle represents the experimental value.

VIII. CONCLUSIONS

We have performed a detailed study of the electromagnetic nucleon form factors within quenched lattice QCD employing a fully non-perturbative $O(a)$-improvement of the fermionic action and of the electromagnetic current. Compared with previous studies [4, 5] we have accumulated much higher statistics, yet our statistical errors appear to be rather large. While these older investigations used one lattice spacing only, we have data at three different lattice spacings. So we could study the discretization errors and found them to be small.

As the quark masses in our simulations are considerably larger than in reality, we had to deal with chiral extrapolations. The most effective way to handle this problem proceeds via a suitable parametrization of the Q^2 dependence of the form factors. Indeed, our data can be described reasonably well by dipole fits. Then the quark-mass dependence of the fit parameters (dipole masses, in particular) can be studied. Assuming a linear dependence on the pion mass one ends up remarkably close to the physical values, in spite of the fact that

the singularities arising from the Goldstone bosons of QCD must show up at some point invalidating such a simple picture. Nevertheless, the difference between the electric and the magnetic dipole mass which we obtain at the physical pion mass is in (semi-quantitative) agreement with recent experimental results [2, 3].

Ideally, the chiral extrapolation should be guided by ChEFT. However, most of the existing chiral expansions do not take into account quenching artefacts and are therefore, strictly speaking, not applicable to our data. But first simulations with dynamical quarks indicate that at the quark masses considered in this paper quenching effects are small so that quenched chiral perturbation theory is not required. While in this respect the size of our quark masses might be helpful, it leads on the other hand to doubts on the applicability of ChEFT. Indeed, only a reorganisation of the standard chiral perturbation theory series allowed Hemmert and Weise [24] to describe with a single expression the phenomenological value of the isovector anomalous magnetic moment of the nucleon as well as (quenched) lattice data. For a different approach to the same problem see Refs. [25, 26, 28].

We have extended the analysis of the magnetic moments of the nucleon of Ref. [24] to the general case of nucleon electromagnetic form factors. Given that these calculations are reliable only for $Q^2 < 0.4\,\mathrm{GeV}^2$, no direct comparison with our lattice data, taken at higher values of Q^2, could be performed. Instead we have converted the dipole masses extracted from our simulations into form factor radii, which could then be compared with the ChEFT formulae. Larger lattices allowing smaller values of Q^2 would be required, if one aims at a direct comparison with the ChEFT results for the form factors.

As low-order (one-loop) ChEFT is insufficient to *simultaneously* account for the quark-mass dependence of the nucleon mass and the form factors in the current matrix elements, we were forced to "normalize" the magnetic moments computed on the lattice before fitting them with the ChEFT formulae. Higher-order calculations in ChEFT, at least at the two-loop level, would be required to avoid this necessity.

In the isovector channel a combined fit of $\kappa_v(m_\pi)$ and the Pauli radius $r_2^v(m_\pi)$ yielded extrapolation functions which describe the lattice data quite well and extrapolate (albeit with large error bar) close to the physical point. For the isovector Dirac radius $r_1^v(m_\pi)$ no chiral extrapolation function could be obtained that is consistent both with the lattice data and known phenomenology at the physical point. Further studies are needed to resolve this discrepancy, both in ChEFT regarding higher order corrections and on the simulation side

investigating quenching effects. (For an alternative view see Ref. [27].) The parameters obtained in the fits are well consistent with those found in Ref. [24]. In particular, we find $\kappa_v^0 = 5.1 \pm 0.8$ as the chiral limit value for the isovector anomalous magnetic moment of the nucleon.

The isoscalar sector is plagued by large uncertainties in the lattice data. The chiral dynamics contributing to extrapolation functions in this sector seems to be dominated by analytic terms. Quantitative studies can only be performed once the statistics of the data is improved and disconnected contributions are taken into account. The ratio κ_p/κ_n could be well described by our chiral extrapolation and was found in remarkable agreement with the constituent quark model.

The leading one-loop calculation in the SSE is found to describe the quark-mass dependence of magnetic quantities quite well. Unfortunately, at the moment we do not have a ChEFT with appropriate counting scheme that simultaneously describes the quark-mass dependence in all four quantities κ_v, κ_s, r_1^v, r_2^v at leading one-loop order. It remains to be seen whether the discrepancies found in $r_1^v(m_\pi)$ can be resolved in a next-to-leading one-loop SSE calculation of the form factors. The figures in this paper show that ChEFT often predicts large effects at values of m_π lighter than those we used in our lattice simulations. In order to confirm the predictions of ChEFT, and in order to extrapolate reliably to physical quark masses, we need simulations at much smaller values of m_π. Moreover, it would be desirable to compute the quark-line disconnected contributions. Important progress is also to be expected from the ongoing simulations with dynamical fermions.

Acknowledgments

This work has been supported in part by the European Community's Human Potential Program under contract HPRN-CT-2000-00145, Hadrons/Lattice QCD, by the DFG (Forschergruppe Gitter-Hadronen-Phänomenologie) and by the BMBF. Discussions with V. Braun and W. Weise are gratefully acknowledged, as well as the constructive remarks of the referee. TRH thanks the Institute for Theoretical Physics of the University of Regensburg and DESY Zeuthen for their kind hospitality.

The numerical calculations were performed on the APE100 at NIC (Zeuthen) as well as on the Cray T3E at ZIB (Berlin) and NIC (Jülich). We wish to thank all institutions for

their support.

APPENDIX A

Here we want to present the nucleon mass as a function of the pion mass in the same formalism that is used for the electromagnetic form factors, i.e. in the SSE to $\mathcal{O}(\epsilon^3)$. The corresponding diagrams are shown in Fig. 15. One finds

$$M_N = M_N^0 - 4c_1 m_\pi^2 - \frac{3g_A^2}{32\pi F_\pi^2} m_\pi^3$$
$$- \frac{c_A^2}{3\pi^2 F_\pi^2}\left\{(\Delta^2 - m_\pi^2)^{3/2}\log R(m_\pi) - (\Delta^3 - \frac{3}{2}\Delta m_\pi^2)\log\left[\frac{2\Delta}{m_\pi}\right] + \frac{1}{4}\Delta m_\pi^2\right\} - 4e_1 m_\pi^4\,, \quad \text{(A1)}$$

where

$$R(m) = \frac{\Delta}{m} + \sqrt{\frac{\Delta^2}{m^2} - 1}\,. \quad \text{(A2)}$$

In (A1) the leading correction to the nucleon mass in the chiral limit M_N^0 is parametrized by the coupling c_1, F_π denotes the pion decay constant, c_A the leading axial $N\Delta$ coupling, g_A the axial coupling of the nucleon, Δ the $\Delta(1232)$-nucleon mass splitting, and e_1 is a counterterm. Eq. (A1) generalizes the analysis of Ref. [7] performed in heavy-baryon chiral perturbation theory to the SSE with dimensional regularization. The expected range of applicability, as reported in Ref. [7], is therefore $m_\pi < 600\,\mathrm{MeV}$.

In Fig. 1 we have used $M_N^0 = 0.88\,\mathrm{GeV}$, $c_1 = -0.93\,\mathrm{GeV}^{-1}$, $g_A = 1.2$, $e_1 = -2.2\,\mathrm{GeV}^{-3}$, in accordance with phenomenological estimates. The remaining parameters have been fixed at their physical values given in Table V. This choice leads to a satisfactory description of nucleon mass data from dynamical simulations at (relatively) low quark masses.

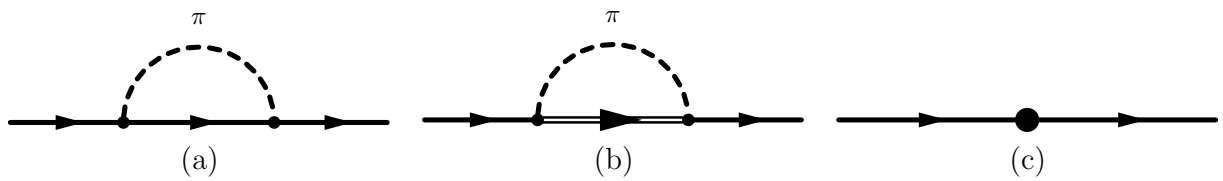

FIG. 15: Diagrams in $\mathcal{O}(\epsilon^3)$ SSE contributing to the nucleon mass.

APPENDIX B

In this Appendix we collect our results for the nucleon form factors.

TABLE VIII: Isovector nucleon form factors at $\beta = 6.0$.

κ	a^2Q^2	G_e	G_m	F_1	F_2
0.1320	0.0000	0.9962(6)		0.9962(6)	
	0.1484	0.554(7)	2.34(4)	0.621(7)	1.72(4)
	0.1492	0.56(2)	2.4(2)	0.63(2)	1.8(2)
	0.2867	0.42(3)	1.69(17)	0.51(3)	1.18(16)
	0.3084	0.357(14)	1.50(8)	0.443(14)	1.06(8)
	0.4168	0.30(5)	1.3(2)	0.40(5)	0.88(18)
	0.4576	0.28(2)	1.13(8)	0.37(2)	0.76(8)
	0.6169	0.141(9)	0.67(4)	0.215(9)	0.45(3)
0.1324	0.0000	0.9936(7)		0.9936(7)	
	0.1480	0.544(7)	2.40(4)	0.619(7)	1.78(4)
	0.1488	0.60(2)	2.6(2)	0.68(2)	1.88(19)
	0.2852	0.40(3)	1.64(16)	0.49(3)	1.15(15)
	0.3084	0.327(14)	1.41(9)	0.415(14)	1.00(8)
	0.4137	0.26(3)	1.39(17)	0.38(4)	1.01(16)
	0.4573	0.27(2)	1.10(9)	0.36(2)	0.73(8)
	0.5350	0.108(18)	0.59(12)	0.17(2)	0.42(11)
	0.6169	0.131(8)	0.69(4)	0.216(9)	0.48(3)
0.1333	0.0000	0.9921(18)		0.9921(18)	
	0.1463	0.503(10)	2.21(6)	0.590(9)	1.62(5)
	0.1477	0.58(4)	2.6(4)	0.68(4)	2.0(4)
	0.2796	0.37(4)	1.5(2)	0.48(4)	1.0(2)
	0.3084	0.28(2)	1.21(12)	0.38(2)	0.83(11)
	0.4029		1.3(2)		
	0.4561	0.24(5)	1.02(15)	0.35(4)	0.67(13)
	0.6169	0.099(11)	0.59(5)	0.191(13)	0.40(4)
0.1338	0.0000	0.999(4)		0.999(4)	
	0.1447	0.475(14)	1.94(8)	0.566(14)	1.38(8)
	0.2741	0.30(6)	0.8(2)	0.36(6)	0.5(2)
	0.3084	0.28(3)	1.17(16)	0.39(3)	0.78(14)
	0.6169	0.12(2)	0.49(6)	0.20(2)	0.29(5)
0.1342	0.0000	0.987(6)		0.987(6)	
	0.1439	0.437(17)	1.91(9)	0.535(17)	1.38(9)
	0.3084	0.26(4)	0.98(17)	0.35(4)	0.62(15)
	0.6169		0.49(8)		

TABLE IX: Isovector nucleon form factors at $\beta = 6.2$.

κ	a^2Q^2	G_e	G_m	F_1	F_2
0.1333	0.0000	1.0010(2)		1.0010(2)	
	0.0665	0.621(7)	3.03(5)	0.692(7)	2.34(5)
	0.0667	0.615(18)	2.90(17)	0.683(18)	2.21(16)
	0.1294	0.413(18)	2.03(11)	0.504(18)	1.52(10)
	0.1371	0.407(15)	2.04(10)	0.504(15)	1.53(10)
	0.1892	0.34(4)	1.62(17)	0.44(4)	1.18(16)
	0.2038	0.32(2)	1.58(8)	0.43(2)	1.15(8)
	0.2742	0.206(10)	1.10(5)	0.306(11)	0.79(5)
0.1339	0.0000	1.0009(3)		1.0009(3)	
	0.0661	0.597(7)	2.77(5)	0.676(7)	2.10(5)
	0.0664	0.64(2)	2.7(2)	0.71(2)	2.0(2)
	0.1279	0.44(3)	2.0(2)	0.55(3)	1.50(19)
	0.1371	0.406(16)	1.84(9)	0.510(16)	1.34(8)
	0.2035	0.32(2)	1.34(9)	0.43(2)	0.92(8)
	0.2742	0.176(11)	0.95(5)	0.279(12)	0.67(4)
0.1344	0.0000	1.0031(7)		1.0031(7)	
	0.0655	0.562(11)	2.74(7)	0.658(11)	2.08(7)
	0.0660	0.56(4)	2.8(3)	0.66(4)	2.1(3)
	0.1259	0.35(3)	1.64(15)	0.46(3)	1.19(14)
	0.1371	0.35(2)	1.65(14)	0.46(2)	1.19(13)
	0.2031	0.28(4)	1.43(14)	0.43(3)	1.00(12)
	0.2742	0.162(15)	0.87(7)	0.277(17)	0.59(6)
0.1349	0.0000	1.0052(18)		1.0052(18)	
	0.0647	0.525(12)	2.44(7)	0.631(12)	1.81(7)
	0.0654	0.55(5)	2.8(4)	0.67(5)	2.1(4)
	0.1233	0.30(4)	1.44(19)	0.42(4)	1.02(18)
	0.1371	0.31(3)	1.41(14)	0.44(3)	0.97(13)
	0.2025	0.26(4)	1.24(14)	0.42(4)	0.82(13)
	0.2742	0.123(18)	0.75(7)	0.25(2)	0.51(6)

TABLE X: Isovector nucleon form factors at $\beta = 6.4$.

κ	a^2Q^2	G_e	G_m	F_1	F_2
0.1338	0.0000	1.0019(18)		1.0019(18)	
	0.0375	0.636(6)	3.10(5)	0.705(6)	2.40(5)
	0.0376	0.626(16)	3.05(14)	0.693(16)	2.36(14)
	0.0730	0.413(18)	1.95(10)	0.494(18)	1.45(10)
	0.0771	0.416(13)	2.10(8)	0.510(13)	1.59(7)
	0.1069	0.29(2)	1.34(9)	0.37(2)	0.97(9)
	0.1147	0.30(2)	1.48(7)	0.397(19)	1.09(7)
	0.1394	0.21(2)	1.00(14)	0.29(2)	0.71(13)
	0.1542	0.215(11)	1.13(5)	0.311(11)	0.82(5)
0.1342	0.0000	1.002(5)		1.002(5)	
	0.0373	0.611(11)	3.01(8)	0.689(11)	2.32(7)
	0.0374	0.61(3)	3.0(2)	0.69(3)	2.3(2)
	0.0724	0.44(4)	2.2(2)	0.55(4)	1.7(2)
	0.0771	0.38(2)	2.05(14)	0.49(2)	1.56(13)
	0.1145	0.26(3)	1.38(11)	0.36(3)	1.02(11)
	0.1542	0.171(19)	0.93(8)	0.26(2)	0.66(8)
0.1346	0.0000	1.003(5)		1.003(5)	
	0.0370	0.576(10)	2.77(6)	0.665(10)	2.11(6)
	0.0372	0.54(3)	2.8(3)	0.63(3)	2.1(3)
	0.0713	0.34(3)	1.53(13)	0.43(3)	1.10(12)
	0.0771	0.347(19)	1.71(10)	0.457(19)	1.25(9)
	0.1034	0.23(4)	1.09(14)	0.32(4)	0.76(13)
	0.1143	0.28(4)	1.24(10)	0.39(4)	0.85(10)
	0.1338	0.16(4)	0.71(14)	0.23(4)	0.48(13)
	0.1542	0.163(14)	0.90(6)	0.273(15)	0.63(5)
0.1350	0.0000	1.006(8)		1.006(8)	
	0.0366	0.531(12)	2.60(8)	0.636(12)	1.97(7)
	0.0369	0.48(5)	2.6(4)	0.59(6)	2.0(4)
	0.0700	0.32(4)	1.57(19)	0.44(4)	1.13(18)
	0.0771	0.29(3)	1.58(15)	0.42(3)	1.16(13)
	0.1009		1.2(3)		
	0.1140	0.26(5)	1.11(12)	0.38(5)	0.73(11)
	0.1298		0.69(17)		
	0.1542	0.142(17)	0.78(6)	0.259(18)	0.53(5)
0.1353	0.0000	1.006(7)		1.006(7)	
	0.0360	0.48(2)	2.22(14)	0.59(2)	1.63(13)
	0.0681		1.5(3)		
	0.0771	0.24(5)	1.39(18)	0.39(5)	1.00(17)
	0.1542		0.73(11)		

TABLE XI: Proton form factors at $\beta = 6.0$.

κ	a^2Q^2	G_e	G_m	F_1	F_2
0.1320	0.0000	0.9980(5)		0.9980(5)	
	0.1484	0.566(6)	1.43(3)	0.599(6)	0.83(3)
	0.1492	0.58(2)	1.49(13)	0.61(2)	0.88(13)
	0.2867	0.42(2)	1.02(10)	0.47(2)	0.56(10)
	0.3084	0.372(12)	0.91(5)	0.413(11)	0.50(5)
	0.4168	0.34(5)	0.77(12)	0.38(4)	0.39(12)
	0.4576	0.287(19)	0.70(5)	0.332(18)	0.37(5)
	0.6169	0.153(8)	0.41(2)	0.190(7)	0.22(2)
0.1324	0.0000	0.9964(6)		0.9964(6)	
	0.1480	0.557(6)	1.47(3)	0.594(5)	0.87(3)
	0.1488	0.600(19)	1.59(13)	0.640(19)	0.95(13)
	0.2852	0.40(2)	1.02(10)	0.45(2)	0.57(9)
	0.3084	0.340(11)	0.88(5)	0.384(11)	0.49(5)
	0.4137	0.29(3)	0.84(10)	0.34(3)	0.49(10)
	0.4573	0.267(18)	0.68(6)	0.315(17)	0.37(5)
	0.5350	0.118(17)	0.37(8)	0.152(18)	0.22(7)
	0.6169	0.143(7)	0.43(2)	0.187(7)	0.24(2)
0.1333	0.0000	0.9957(13)		0.9957(13)	
	0.1463	0.517(8)	1.36(3)	0.560(8)	0.80(3)
	0.1477	0.57(3)	1.6(2)	0.62(3)	1.0(2)
	0.2796	0.39(3)	0.91(14)	0.44(3)	0.47(13)
	0.3084	0.294(15)	0.76(7)	0.342(15)	0.42(7)
	0.4029	0.27(5)	0.81(15)	0.34(5)	0.47(14)
	0.4561	0.26(4)	0.66(9)	0.32(3)	0.34(9)
	0.6169	0.113(9)	0.37(3)	0.161(9)	0.21(3)
0.1338	0.0000	1.000(3)		1.000(3)	
	0.1447	0.488(12)	1.21(5)	0.532(11)	0.67(5)
	0.2741	0.30(5)	0.54(15)	0.32(5)	0.22(14)
	0.3084	0.30(2)	0.74(10)	0.35(2)	0.39(9)
	0.6169	0.125(17)	0.31(4)	0.166(16)	0.14(3)
0.1342	0.0000	0.994(5)		0.994(5)	
	0.1439	0.451(13)	1.17(6)	0.499(13)	0.68(6)
	0.3084	0.25(3)	0.62(11)	0.30(3)	0.32(10)
	0.6169	0.094(19)	0.31(5)	0.145(19)	0.17(4)

TABLE XII: Proton form factors at $\beta = 6.2$.

κ	a^2Q^2	G_e	G_m	F_1	F_2
0.1333	0.0000	1.00196(17)		1.00196(17)	
	0.0665	0.633(5)	1.85(3)	0.669(5)	1.18(3)
	0.0667	0.626(15)	1.82(11)	0.662(15)	1.16(10)
	0.1294	0.426(15)	1.24(7)	0.472(15)	0.77(6)
	0.1371	0.423(12)	1.24(6)	0.471(12)	0.77(6)
	0.1892	0.37(4)	1.00(11)	0.42(4)	0.58(10)
	0.2038	0.333(18)	0.97(5)	0.387(17)	0.58(5)
	0.2742	0.219(10)	0.67(3)	0.269(9)	0.40(3)
0.1339	0.0000	1.0020(3)		1.0020(3)	
	0.0661	0.607(6)	1.70(3)	0.646(6)	1.05(3)
	0.0664	0.637(19)	1.71(13)	0.676(19)	1.04(12)
	0.1279	0.45(3)	1.22(12)	0.50(3)	0.72(12)
	0.1371	0.414(13)	1.13(6)	0.466(13)	0.66(5)
	0.2035	0.33(2)	0.83(5)	0.380(19)	0.45(5)
	0.2742	0.184(10)	0.58(3)	0.237(9)	0.34(3)
0.1344	0.0000	1.0037(5)		1.0037(5)	
	0.0655	0.576(8)	1.67(4)	0.624(8)	1.05(4)
	0.0660	0.56(3)	1.8(2)	0.62(3)	1.1(2)
	0.1259	0.37(2)	1.02(9)	0.42(2)	0.60(9)
	0.1371	0.368(18)	1.00(8)	0.424(18)	0.57(8)
	0.1823	0.29(7)			
	0.2031	0.30(3)	0.88(8)	0.38(3)	0.50(8)
	0.2742	0.174(13)	0.53(4)	0.232(13)	0.30(4)
0.1349	0.0000	1.0054(12)		1.0054(12)	
	0.0647	0.535(9)	1.49(5)	0.588(9)	0.91(4)
	0.0654	0.55(4)	1.8(3)	0.62(4)	1.2(3)
	0.1233	0.34(3)	0.86(12)	0.39(3)	0.47(11)
	0.1371	0.34(2)	0.85(8)	0.392(19)	0.46(8)
	0.2025	0.27(4)	0.76(9)	0.34(3)	0.41(8)
	0.2742	0.133(13)	0.47(4)	0.199(13)	0.27(3)

TABLE XIII: Proton form factors at $\beta = 6.4$.

κ	a^2Q^2	G_e	G_m	F_1	F_2
0.1338	0.0000	1.0024(14)		1.0024(14)	
	0.0375	0.644(5)	1.89(3)	0.679(5)	1.21(3)
	0.0376	0.641(13)	1.89(9)	0.676(13)	1.21(9)
	0.0730	0.421(16)	1.19(6)	0.462(16)	0.73(6)
	0.0771	0.430(11)	1.30(5)	0.479(11)	0.82(5)
	0.1069	0.30(2)	0.82(6)	0.34(2)	0.48(6)
	0.1147	0.311(17)	0.91(5)	0.359(16)	0.55(4)
	0.1394	0.22(2)	0.61(9)	0.25(2)	0.36(8)
	0.1542	0.225(10)	0.69(3)	0.274(9)	0.42(3)
0.1342	0.0000	1.002(4)		1.002(4)	
	0.0373	0.622(9)	1.84(4)	0.661(9)	1.18(4)
	0.0374	0.60(2)	1.86(15)	0.65(2)	1.22(15)
	0.0724	0.45(3)	1.38(14)	0.50(3)	0.88(13)
	0.0771	0.398(19)	1.26(9)	0.454(19)	0.81(8)
	0.1145	0.27(3)	0.84(7)	0.32(2)	0.52(7)
	0.1542	0.186(17)	0.58(5)	0.234(16)	0.34(5)
0.1346	0.0000	1.003(3)		1.003(3)	
	0.0370	0.588(8)	1.70(4)	0.632(7)	1.06(4)
	0.0372	0.58(2)	1.72(17)	0.62(2)	1.10(17)
	0.0713	0.35(2)	0.95(8)	0.40(2)	0.55(8)
	0.0771	0.368(15)	1.07(6)	0.425(14)	0.65(6)
	0.1034	0.24(4)	0.67(9)	0.29(3)	0.38(8)
	0.1143	0.28(3)	0.76(7)	0.34(3)	0.42(7)
	0.1338	0.16(2)	0.44(9)	0.19(2)	0.24(8)
	0.1542	0.175(12)	0.55(4)	0.232(11)	0.32(3)
0.1350	0.0000	1.004(6)		1.004(6)	
	0.0366	0.549(10)	1.60(5)	0.602(9)	1.00(5)
	0.0369	0.53(4)	1.6(3)	0.59(4)	1.0(3)
	0.0700	0.32(3)	1.00(12)	0.38(3)	0.61(11)
	0.0771	0.319(19)	0.99(9)	0.387(19)	0.61(9)
	0.1009	0.21(4)	0.74(18)	0.27(4)	0.47(16)
	0.1140	0.27(4)	0.64(8)	0.32(4)	0.32(8)
	0.1298		0.41(10)		
	0.1542	0.150(13)	0.48(4)	0.210(13)	0.27(3)
0.1353	0.0000	1.002(5)		1.002(5)	
	0.0360	0.474(17)	1.38(9)	0.533(17)	0.85(8)
	0.0681	0.32(6)	1.0(2)	0.40(6)	0.6(2)
	0.0771	0.28(4)	0.85(11)	0.35(3)	0.50(10)
	0.1542	0.15(3)	0.48(7)	0.23(3)	0.25(6)

TABLE XIV: Magnetic form factor of the neutron at $\beta = 6.0$.

κ	a^2Q^2	G_m
0.1320	0.1484	−0.908(18)
	0.2867	−0.67(7)
	0.3084	−0.58(3)
	0.4168	−0.50(8)
	0.4576	−0.42(4)
	0.6169	−0.256(14)
0.1324	0.1480	−0.928(17)
	0.1488	−1.01(11)
	0.2852	−0.62(6)
	0.3084	−0.53(4)
	0.4137	−0.55(7)
	0.4573	−0.40(4)
	0.5350	−0.21(5)
	0.6169	−0.264(15)
0.1333	0.1463	−0.85(2)
	0.2796	−0.55(9)
	0.3084	−0.45(5)
	0.4029	−0.53(10)
	0.6169	−0.220(18)
0.1338	0.1447	−0.74(3)
	0.3084	−0.44(7)
	0.6169	−0.18(3)
0.1342	0.1439	−0.73(4)
	0.3084	−0.36(7)
	0.6169	−0.18(3)

TABLE XV: Magnetic form factor of the neutron at $\beta = 6.2$.

κ	a^2Q^2	G_m
0.1333	0.0665	−1.186(19)
	0.0667	−1.10(8)
	0.1294	−0.79(4)
	0.1371	−0.80(4)
	0.1892	−0.61(7)
	0.2742	−0.43(2)
0.1339	0.0661	−1.07(2)
	0.1279	−0.83(8)
	0.1371	−0.71(4)
	0.2742	−0.37(2)
0.1344	0.0655	−1.07(3)
	0.1259	−0.62(6)
	0.1371	−0.65(6)
	0.2742	−0.34(3)
0.1349	0.0647	−0.94(3)
	0.1233	−0.58(9)
	0.1371	−0.55(6)
	0.2742	−0.29(3)

TABLE XVI: Magnetic form factor of the neutron at $\beta = 6.4$.

κ	a^2Q^2	G_m
0.1338	0.0375	−1.208(19)
	0.0376	−1.20(7)
	0.0730	−0.75(4)
	0.0771	−0.80(3)
	0.1069	−0.53(4)
	0.1394	−0.39(6)
	0.1542	−0.44(2)
0.1342	0.0373	−1.17(3)
	0.0724	−0.81(9)
	0.0771	−0.79(6)
	0.1542	−0.35(3)
0.1346	0.0370	−1.07(3)
	0.0713	−0.58(5)
	0.0771	−0.64(4)
	0.1034	−0.42(5)
	0.1338	−0.28(6)
	0.1542	−0.35(2)
0.1350	0.0366	−1.00(3)
	0.0700	−0.58(8)
	0.0771	−0.59(6)
	0.1009	−0.44(11)
	0.1140	−0.37(6)
	0.1542	−0.31(2)
0.1353	0.0360	−0.85(6)
	0.0681	−0.52(12)
	0.0771	−0.55(9)
	0.1542	−0.25(4)

APPENDIX C

The following tables contain the results of our dipole fits. The masses are given in lattice units.

TABLE XVII: Dipole fits of the isovector form factors.

κ	aM_e	A_m	aM_m	aM_1	A_2	aM_2
			$\beta = 6.0$			
0.1320	0.657(6)	4.3(2)	0.66(2)	0.756(7)	3.4(2)	0.61(3)
0.1324	0.637(5)	4.5(2)	0.64(2)	0.745(7)	3.6(2)	0.60(3)
0.1333	0.593(8)	4.3(3)	0.61(3)	0.705(9)	3.5(4)	0.56(4)
0.1338	0.570(12)	4.1(6)	0.57(5)	0.675(14)	3.4(7)	0.50(6)
0.1342	0.534(14)	4.0(7)	0.57(7)	0.633(17)	4.(2)	0.44(15)
			$\beta = 6.2$			
0.1333	0.493(4)	4.79(17)	0.507(16)	0.579(5)	3.87(18)	0.480(19)
0.1339	0.477(5)	4.6(2)	0.484(17)	0.566(6)	3.7(2)	0.45(2)
0.1344	0.441(6)	4.7(3)	0.46(2)	0.539(8)	3.9(4)	0.42(3)
0.1349	0.411(7)	4.3(3)	0.45(3)	0.511(9)	3.5(4)	0.41(3)
			$\beta = 6.4$			
0.1338	0.375(3)	5.16(18)	0.358(10)	0.436(4)	4.19(19)	0.340(12)
0.1342	0.358(5)	5.2(3)	0.347(17)	0.422(7)	4.2(3)	0.33(2)
0.1346	0.333(4)	5.1(3)	0.322(14)	0.399(5)	4.2(3)	0.299(16)
0.1350	0.310(5)	4.8(4)	0.319(16)	0.384(7)	3.9(4)	0.30(2)
0.1353	0.282(11)	3.7(5)	0.35(4)	0.350(14)	2.9(9)	0.33(9)

TABLE XVIII: Dipole fits of the proton form factors.

κ	aM_e	A_m	aM_m	aM_1	A_2	aM_2
			$\beta = 6.0$			
0.1320	0.673(5)	2.59(12)	0.66(2)	0.720(5)	1.62(14)	0.61(4)
0.1324	0.653(5)	2.71(13)	0.64(2)	0.706(5)	1.70(14)	0.61(3)
0.1333	0.608(6)	2.59(18)	0.62(3)	0.665(7)	1.61(19)	0.59(5)
0.1338	0.583(10)	2.5(3)	0.58(5)	0.635(10)	1.7(5)	0.51(8)
0.1342	0.543(11)	2.4(4)	0.59(7)	0.596(11)	1.5(4)	0.55(10)
			$\beta = 6.2$			
0.1333	0.505(4)	2.93(10)	0.505(16)	0.547(4)	1.97(12)	0.48(2)
0.1339	0.485(4)	2.81(12)	0.483(17)	0.527(4)	1.83(13)	0.45(3)
0.1344	0.453(5)	2.87(19)	0.46(2)	0.501(6)	2.0(2)	0.42(3)
0.1349	0.420(5)	2.6(2)	0.44(3)	0.469(6)	1.7(2)	0.41(4)
			$\beta = 6.4$			
0.1338	0.383(3)	3.15(11)	0.359(10)	0.412(3)	2.13(12)	0.340(15)
0.1342	0.366(4)	3.17(19)	0.349(17)	0.398(5)	2.1(2)	0.33(2)
0.1346	0.342(3)	3.08(18)	0.325(14)	0.374(4)	2.1(2)	0.30(2)
0.1350	0.319(4)	3.0(2)	0.314(16)	0.356(4)	2.0(3)	0.29(2)
0.1353	0.287(7)	2.2(3)	0.36(4)	0.326(8)	1.5(4)	0.33(5)

TABLE XIX: Dipole fits of the neutron magnetic form factor.

κ	A_m	aM_m
	$\beta = 6.0$	
0.1320	$-1.68(9)$	0.65(2)
0.1324	$-1.78(9)$	0.62(2)
0.1333	$-1.71(14)$	0.59(3)
0.1338	$-1.6(2)$	0.57(6)
0.1342	$-1.6(3)$	0.55(7)
	$\beta = 6.2$	
0.1333	$-1.90(8)$	0.498(18)
0.1339	$-1.78(9)$	0.48(2)
0.1344	$-1.90(15)$	0.44(3)
0.1349	$-1.70(16)$	0.43(3)
	$\beta = 6.4$	
0.1338	$-2.05(8)$	0.351(11)
0.1342	$-2.06(16)$	0.34(2)
0.1346	$-2.01(14)$	0.314(15)
0.1350	$-1.84(16)$	0.319(19)
0.1353	$-1.5(2)$	0.32(4)

[1] H.-Y. Gao, Int. J. Mod. Phys. E **12**, 1 (2003).

[2] M.K. Jones et al., Phys. Rev. Lett. **84**, 1398 (2000).

[3] O. Gayou et al., Phys. Rev. C **64**, 038202 (2001).

[4] T. Draper, R.M. Woloshyn, and K.F. Liu, Phys. Lett. B **234**, 121 (1990); D.B. Leinweber, R.M. Woloshyn, and T. Draper, Phys. Rev. D **43**, 1659 (1991); W. Wilcox, T. Draper, and K.F. Liu, Phys. Rev. D **46**, 1109 (1992).

[5] V. Gadiyak, X. Ji, and C. Jung, Phys. Rev. D **65**, 094510 (2002); see however: W. Wilcox, Phys. Rev. D **66**, 017502 (2002).

[6] M. Lüscher, S. Sint, R. Sommer, P. Weisz, and U. Wolff, Nucl. Phys. **B491**, 323 (1997).

[7] V. Bernard, T.R. Hemmert, and U.-G. Meißner, Nucl. Phys. **A732**, 149 (2004).

[8] D.B. Leinweber, A.W. Thomas, and R.D. Young, Phys. Rev. Lett. **92**, 242002 (2004).

[9] D. Pleiter, Thesis, Freie Universität Berlin (2000).

[10] R. Sommer, Nucl. Phys. **B411**, 839 (1994).

[11] M. Guagnelli, R. Sommer, and H. Wittig, Nucl. Phys. **B535**, 389 (1998).

[12] C. Best, M. Göckeler, R. Horsley, E.-M. Ilgenfritz, H. Perlt, P. Rakow, A. Schäfer, G. Schierholz, A. Schiller, and S. Schramm, Phys. Rev. D **56**, 2743 (1997).

[13] M. Lüscher, S. Sint, R. Sommer, and H. Wittig, Nucl. Phys. **B491**, 344 (1997).

[14] T. Bakeyev, M. Göckeler, R. Horsley, D. Pleiter, P.E.L. Rakow, A. Schäfer, G. Schierholz, and H. Stüben, Nucl. Phys. Proc. Suppl. **119**, 467 (2003); T. Bakeyev, M. Göckeler, R. Horsley, D. Pleiter, P.E.L. Rakow, G. Schierholz, and H. Stüben Phys. Lett. B **580**, 197 (2004).

[15] M. Guagnelli and R. Sommer, Nucl. Phys. Proc. Suppl. **63**, 886 (1998); R. Sommer, private communication; S. Capitani, M. Göckeler, R. Horsley, H. Oelrich, H. Perlt, D. Pleiter, P.E.L. Rakow, G. Schierholz, A. Schiller, and P. Stephenson, Nucl. Phys. Proc. Suppl. **63**, 233, 871 (1998).

[16] S. Sint and P. Weisz, Nucl. Phys. **B502**, 251 (1997); S. Capitani, M. Göckeler, R. Horsley, H. Perlt, P.E.L. Rakow, G. Schierholz, and A. Schiller, Nucl. Phys. **B593**, 183 (2001).

[17] K.F. Liu, J. Phys. G **27**, 511 (2001) and references therein.

[18] S.J. Dong, K.F. Liu, and A.G. Williams, Phys. Rev. D **58**, 074504 (1998); A.G. Williams, Nucl. Phys. Proc. Suppl. **73**, 306 (1999); N. Mathur and S.J. Dong, Nucl. Phys. Proc. Suppl.

94, 311 (2001); W. Wilcox, Nucl. Phys. Proc. Suppl. **94**, 319 (2001).

[19] R. Lewis, W. Wilcox, and R.M. Woloshyn, Phys. Rev. D **67**, 013003 (2003).

[20] A. Tang, W. Wilcox, and R. Lewis, Phys. Rev. D **68**, 094503 (2003).

[21] S. Capitani, M. Göckeler, R. Horsley, B. Klaus, H. Oelrich, H. Perlt, D. Petters, D. Pleiter, P.E.L. Rakow, G. Schierholz, A. Schiller, and P. Stephenson, Nucl. Phys. Proc. Suppl. **73**, 294 (1999).

[22] M. Göckeler, R. Horsley, D. Pleiter, P.E.L. Rakow, and G. Schierholz, in: *Lepton Scattering, Hadrons and QCD*, eds. W. Melnitchouk, A.W. Schreiber, A.W. Thomas, and P.C. Tandy (World Scientific, Singapore, 2001), hep-ph/0108105.

[23] C. Bernard, S. Hashimoto, D.B. Leinweber, P. Lepage, E. Pallante, S.R. Sharpe, and H. Wittig, Nucl. Phys. Proc. Suppl. **119**, 170 (2003) and references therein.

[24] T.R. Hemmert and W. Weise, Eur. Phys. J. A **15**, 487 (2002).

[25] D.B. Leinweber, D.H. Lu, and A.W. Thomas, Phys. Rev. D **60**, 034014 (1999).

[26] D.B. Leinweber, A.W. Thomas, and R.D. Young, Phys. Rev. Lett. **86**, 5011 (2001).

[27] E.J. Hackett-Jones, D.B. Leinweber, and A.W. Thomas, Phys. Lett. B **494**, 89 (2000); G.V. Dunne, A.W. Thomas, and S.V. Wright, Phys. Lett. B **531**, 77 (2002).

[28] J.D. Ashley, D.B. Leinweber, A.W. Thomas, and R.D. Young, Eur. Phys. J. A **19**, 9 (2004).

[29] V. Bernard, H.W. Fearing, T.R. Hemmert, and U.-G. Meißner, Nucl. Phys. **A635**, 121 (1998); **A642**, 563(E) (1998).

[30] P. Mergell, U.-G. Meißner, and D. Drechsel, Nucl. Phys. **A596**, 367 (1996).

[31] T.R. Hemmert, B.R. Holstein, and J. Kambor, J. Phys. G **24**, 1831 (1998).

[32] B. Kubis and U.-G. Meißner, Nucl. Phys. **A679**, 698 (2001).

[33] N. Fettes, U.-G. Meißner, M. Mojžiš, and S. Steininger, Ann. Phys. **283**, 273 (2000); **288**, 249(E) (2001).

[34] D.B. Leinweber, Nucl. Phys. Proc. Suppl. **109A**, 45 (2002); D.B. Leinweber, Phys. Rev. D **69**, 014005 (2004); M.J. Savage, Nucl. Phys. **A700**, 359 (2002).

[35] T.R. Hemmert, M. Procura, and W. Weise, Phys. Rev. D **68**, 075009 (2003).

[36] V. Bernard, N. Kaiser, and U.-G. Meißner, Nucl. Phys. **A611**, 429 (1996).